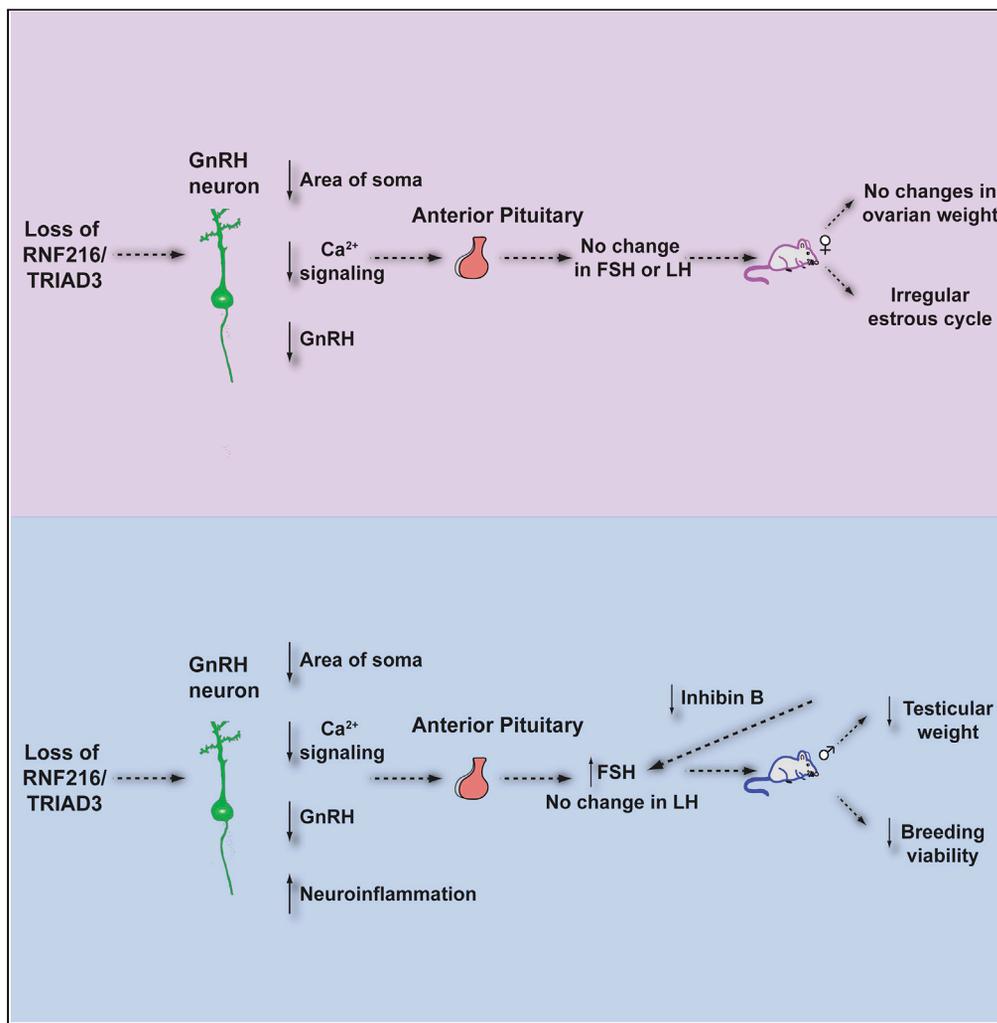# iScience

Article

The E3 ubiquitin ligase RNF216/TRIAD3 is a key coordinator of the hypothalamic-pituitary-gonadal axis

Arlene J. George, Bin Dong, Hannah Lail, ..., Erik Hrabovszky, Desiree Wanders, Angela M. Mabb

amabb@gsu.edu

Highlights

Rnf216/Triad3 controls GnRH production and intrinsic hypothalamic cell activity

Rnf216/Triad3 knockout male mice have greater reproductive impairments than females

Rnf216/Triad3 controls the HPG axis differently in males and females

Rnf216/Triad3 knockout male mice have reactive microglia in the hypothalamus

Article

The E3 ubiquitin ligase RNF216/TRIAD3 is a key coordinator of the hypothalamic-pituitary-gonadal axis

Arlene J. George,[1,2] Bin Dong,[3] Hannah Lail,[4] Morgan Gomez,[1] Yarely C. Hoffiz,[1] Christopher B. Ware,[1] Ning Fang,[5] Anne Z. Murphy,[1] Erik Hrabovszky,[6] Desiree Wanders,[4] and Angela M. Mabb[1,2,7,*]

SUMMARY

Recessive mutations in *RNF216/TRIAD3* cause Gordon Holmes syndrome (GHS), in which dysfunction of the hypothalamic-pituitary-gonadal (HPG) axis and neurodegeneration are thought to be core phenotypes. We knocked out *Rnf216/Triad3* in a gonadotropin-releasing hormone (GnRH) hypothalamic cell line. *Rnf216/Triad3* knockout (KO) cells had decreased steady-state GnRH and calcium transients. *Rnf216/Triad3* KO adult mice had reductions in GnRH neuron soma size and GnRH production without changes in neuron densities. In addition, KO male mice had smaller testicular volumes that were accompanied by an abnormal release of inhibin B and follicle-stimulating hormone, whereas KO females exhibited irregular estrous cycling. KO males, but not females, had reactive microglia in the hypothalamus. Conditional deletion of *Rnf216/Triad3* in neural stem cells caused abnormal microglia expression in males, but reproductive function remained unaffected. Our findings show that dysfunction of RNF216/TRIAD3 affects the HPG axis and microglia in a region- and sex-dependent manner, implicating sex-specific therapeutic interventions for GHS.

INTRODUCTION

The integrity of the hypothalamic-pituitary-gonadal (HPG) axis is necessary for neuroendocrine control of reproductive behavior that is mediated by the secretion of hormones via tightly regulated neural networks (Harris, 1955). Activation of the HPG axis is initiated by a population of kisspeptin neurons in the anteroventral periventricular nucleus (AVPV) and arcuate nucleus (ARN) that release kisspeptin. Kisspeptin then binds to G-protein coupled receptor 54 (GPR54) located on the surface of gonadotropin-releasing hormone (GnRH) neurons in the preoptic area of the hypothalamus (Han et al., 2005; Herbison, 2016). The activation of these receptors facilitates calcium-dependent pathways that are critical for GnRH production and release (Armstrong et al., 2009; Kotani et al., 2001; Moenter et al., 2003). GnRH then stimulates secretory gonadotropes located in the anterior pituitary to release the gonadotropins, luteinizing hormone (LH) and follicle-stimulating hormone (FSH), which act on the gonads to regulate the secretion of sex steroids (Plant, 2015).

Loss-of-function mutations in HPG axis neuropeptides, gonadotropins, and receptor genes cause hypogonadotropic hypogonadism (HH) (Achrekar et al., 2010; Bramble et al., 2016; Bruysters et al., 2008; de Roux et al., 1997, 2003; Seminara et al., 2003). HH is a condition that is defined by gonadal impairments with decreased levels of sex steroids because of HPG axis defects (de Roux et al., 1997; Kalantaridou and Chrousos, 2002). HH is prevalent in a diverse set of disorders that include Kallmann syndrome, Prader-Willi syndrome, Fragile X syndrome, cerebellar ataxias, and central and peripheral hypomyelination (Alsemari, 2013; Angulo et al., 2015; Hardelin, 2001; Timmons et al., 2006). One neurological disease with a defining feature of HH is Gordon Holmes syndrome (GHS), a rare disorder with a constellation of signs and symptoms that also include cerebellar ataxia, dysarthria, cognitive impairment, and neurodegeneration (Holmes, 1908; Seminara et al., 2002). Individuals with GHS are diagnosed around pubertal age and often present with poor development of secondary sexual characteristics concurrent with low levels of LH and testosterone (Alqwaifly and Bohlega, 2016; Ganos et al., 2015; Mehmood et al., 2017; Quinton et al., 1999; Seminara et al., 2002). Clinical studies show that some, but not all GHS patients will respond to

[1]Neuroscience Institute, Georgia State University, 100 Piedmont Avenue, Atlanta, GA 30303, USA

[2]Center for Behavioral Neuroscience, Georgia State University, Atlanta, GA 30303, USA

[3]Department of Chemistry and Biochemistry, University of Arkansas, Fayetteville, AR 72701, USA

[4]Department of Nutrition, Georgia State University, 140 Decatur St SE, Atlanta, GA 30303, USA

[5]Department of Chemistry, Georgia State University, 50 Decatur St SE., Atlanta, GA 30302, United States

[6]Laboratory of Reproductive Neurobiology, Institute of Experimental Medicine, Budapest, Hungary

[7]Lead contact

*Correspondence: amabb@gsu.edu

https://doi.org/10.1016/j.isci. 2022.104386

treatment with exogenous GnRH, but this remains a short-term solution as patient responsiveness wanes over time (Margolin et al., 2013; Quinton et al., 1999; Seminara et al., 2002).

Emerging evidence indicates that protein ubiquitination is critical for HPG axis function. Protein ubiquitination is an ATP-driven posttranslational modification that involves the covalent addition of a small protein called ubiquitin to other proteins, resulting in a multitude of cellular functions (Hershko and Ciechanover, 1998). This is initiated by a ubiquitin-activating enzyme (E1) that transfers the ubiquitin to a ubiquitin-conjugating enzyme (E2), which will then form a complex with a ubiquitin ligase (E3) to transfer ubiquitin to the target protein or substrate (Komander and Rape, 2012; Zheng and Shabek, 2017). Heterozygous mutations in the E3 ligase, makorin RING-finger protein 3 (*MKRN3*), and low serum levels of MKRN3 are linked to central precocious puberty (Aycan et al., 2018; de Vries et al., 2014; Grandone et al., 2018; Liu et al., 2017; Stecchini et al., 2016). Disruptions in protein ubiquitin enzymes are also associated with HH where homozygous recessive or compound heterozygous mutations in the E3 ligases *STUB1/CHIP* or *RNF216/TRIAD3* are causative for GHS (Alqwaifly and Bohlega, 2016; Calandra et al., 2019; Ganos et al., 2015; George et al., 2018; Hayer et al., 2017; Margolin et al., 2013; Mehmood et al., 2017; Santens et al., 2015; Sawyer et al., 2014; Song et al., 2013).

RNF216/TRIAD3 is an RBR (RING-between-RING) E3 ligase that encodes for multiple isoforms that include TRIAD3A, TRIAD3B, TRIAD3C, and TRIAD3D/E (Chuang and Ulevitch, 2004). Notably, TRIAD3A can assemble lysine-48 (-K48) ubiquitin linkages which often lead to proteasome-dependent degradation of multifarious substrates including those involved in immunological function and cell death (Alturki et al., 2018; Chuang and Ulevitch, 2004; Fearns et al., 2006; Nakhaei et al., 2009). RNF216/TRIAD3 also ubiquitinates substrates that regulate autophagy (Kim et al., 2018; Wang et al., 2016; Xu et al., 2014). Recent literature highlights a role for RNF216/TRIAD3 in the assembly of-K63 ubiquitin linkages, which mediate signal transduction processes (Cotton et al., 2022; Schwintzer et al., 2019; Seenivasan et al., 2019). The findings described above have been focused outside of the nervous system. The only documented role of RNF216/TRIAD3 in the nervous system is its regulation in learning-related synaptic plasticity (Mabb et al., 2014). TRIAD3A localizes to clathrin-coated pits and is associated with endocytic zones within the postsynaptic membrane of primary neurons. Triad3A ubiquitinates ARC, an immediate-early gene product that regulates the trafficking of surface α-amino-3-hydroxy-5-methyl-4-isoxazolepropionic acid (AMPA) receptors (Mabb et al., 2014). A loss in Triad3A-dependent ARC ubiquitination increases AMPA receptor endocytosis and prolongs metabotropic glutamate receptor-mediated long-term depression (mGluR-LTD) in hippocampal neurons (Wall et al., 2018). Remarkably, there is limited literature describing a role for *RNF216/TRIAD3* in HH, one of the core phenotypes associated with GHS, nor have there been attempts to dissect the functions of ubiquitin enzymes at multiple levels within the HPG axis.

In this study, we unveiled the role of RNF216/TRIAD3 within the complex HPG axis. Using the CRISPR-Cas9 system, we knocked out *Rnf216/Triad3* isoforms in GT1-7 cells, an immortalized cell line derived from mouse GnRH neurons that secretes GnRH (Mellon et al., 1990) and expresses RNF216/TRIAD3. Deletion of *Rnf216/Triad3* reduced GnRH secretion without changing the expression or localization of GPR54 and GnRH receptors (GnRHR). Using the genetically encoded calcium sensor R-GECO1, we found that *Rnf216/Triad3* knockout (KO) cells exhibited reduced activity. Characterization of *Rnf216/Triad3* KO mice showed deteriorations in reproductive health that included lower breeding viability in males, irregular female estrous cycling, and decreased male gonadal volume. Surprisingly, the downstream GnRH gonadotropin effector, FSH, was increased whereas the negative regulator of FSH, inhibin B, was decreased specifically in males. Unlike KO males, basal gonadotropins were unchanged in female KO mice despite decreased GnRH production and GnRH soma size in both sexes. Although we did not detect changes in brain volume that were indicative of neurodegeneration, adult KO males selectively showed decreased microglia area in the hypothalamus that was accompanied by elevated levels of the microglia-secreted proinflammatory cytokine, interleukin-1beta (IL-1β). Selective deletion of *Rnf216/Triad3* in neural stem cells also caused a reduction in microglia area in males, but the HPG axis was found to be normal in males and females. These findings indicate that the loss of function of *RNF216/TRIAD3* is associated with an impaired neuroendocrine axis, with dysfunction of RNF216/TRIAD3 on HPG axis profiles occurring in a region- and sex-dependent manner.

RESULTS

Rnf216/Triad3 KO GT1-7 cells have decreased GnRH production and calcium transient frequency

Since HH in GHS is manifested by decreased GnRH release (Alqwaifly and Bohlega, 2016; Ganos et al., 2015; Holmes, 1908; Mehmood et al., 2017; Quinton et al., 1999; Seminara et al., 2002) and the presence
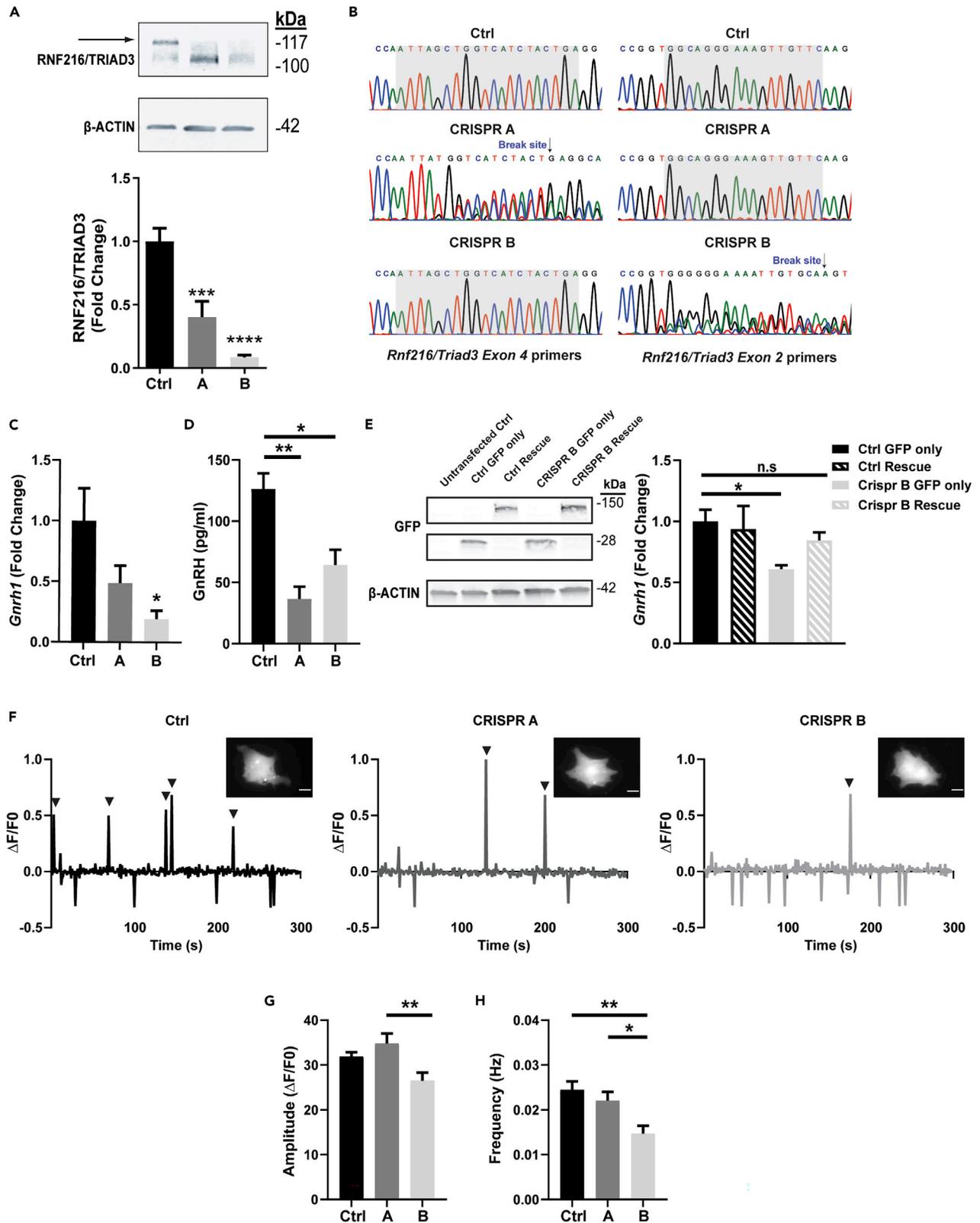
Figure 1. *Rnf216/Triad3* reduces GnRH and Ca^{2+} transient frequency in GT1-7 cells

(A) Generation of *Rnf216/Triad3* hypothalamic GT1-7 knockout cells. *Top*, Representative immunoblot illustrating RNF216/TRIAD3 in CRISPR-Cas9 control (Ctrl) and knockout cells (A and B). *Bottom*, Mean RNF216/TRIAD3 in control and knockout cells. RNF216/TRIAD3 values were normalized to β-ACTIN. (F (2, 15) = 60.31, ****p< 0.0001, One-way ANOVA). Bonferroni's multiple comparisons test shows that CRISPR A (***p = 0.0009) and B (****p<0.0001) are significantly lower than control. N = 6 samples per condition. Error bars are +SEM.

(B) Sanger sequencing demonstrates successful targeting of *Rnf216/Triad3* in CRISPR A (*left*) and B (*right*) with arrows indicating break sites. The highlighted region represents gRNA targeting site/s.

(C) qPCR demonstrating a significant decrease in *Gnrh1* (F (2, 6) = 5.129, *p = 0.05, One-way ANOVA). Bonferroni's multiple comparisons test showed a non-significant reduction in CRISPR A by 51.36% ± 0.1445%, p = 0.1820, and a significant reduction in CRISPR B by 80.82% ± 0.06998%, *p = 0.0389. N = 3 cDNA samples per condition. Error bars are +SEM.

(D) GnRH ELISA depicting reduction in basal GnRH release in CRISPR A and B. F (2,8) =13.97, **p = 0.0025. One-way ANOVA with Dunnett's multiple comparison test. Crispr A was significantly different from the control (**p =0.0014). Crispr B was significantly different than the control (*p = 0.0122). N = 3 samples for Ctrl, N = 4 samples for CRISPR A, and N = 4 samples for CRISPR B. Error bars are +SEM.

(E) *Left*, Representative immunoblots demonstrating expression of GFP-RNF216/TRIAD3 Isoforms A and B transfected in Ctrl and CRISPR B. *Right*, qPCR of *Gnrh1* with Ctrl and B transfected with GFP or GFP-tagged Crispr resistant RNF216/TRIAD3 A and B isoforms (Rescue). CRISPR B Rescue showed no significant differences compared to Ctrl GFP only. CRISPR B with GFP only (*p =0.0418) showed significant differences compared to Ctrl GFP only (F (5,18) = 8.063, **p = 0.0004). N = 4 cDNA samples per condition. Error bars are +SEM.

(F) Calcium signaling in Ctrl and *Rnf216/Triad3* knockout cells. Representative fluorescence intensity plots of CRISPR Ctrl, A, and B. Positive signals were measured as 2 standard deviations above the baseline mean indicated by (▼). *Inset*, Representative fluorescent images from each condition. Scale bars represent 10 μm.

(G) Average amplitude of positive event transients. F (2, 81) = 5.690, **p = 0.0049. One-way ANOVA with Tukey post-hoc analysis. Crispr B was significantly different from Crispr A (**p = 0.0038). Error bars are +SEM.

(H) Frequency of event transients is counted as the total number of positive signals in 300 s. (F (2, 81) = 7.263, **p = 0.0013, One-way ANOVA) with Tukey post-hoc analysis. Crispr B was significantly different than the control (**p = 0.0014) and from Crispr A (*p = 0.0194). N = 28 cells for Ctrl, CRISPR A, and CRISPR B. Error bars are + SEM.

See also Figure S1.

of feedback loops within the HPG axis can alter this release (Plant, 2015), we sought to test the role of RNF216/TRIAD3 in the release of GnRH in GT1-7 cells using loss-of-function experiments. Utilizing the CRISPR-Cas9-mediated knockout strategy (Shalem et al., 2014), we generated two separate gRNA clones (A and B) targeting the *Rnf216/Triad3* gene. Clone A decreased RNF216/TRIAD3 by 63 ± 0.10% whereas clone B yielded a 90 ± 0.03% decrease (p< 0.0001, One-way ANOVA; Figure 1A). Purification of genomic DNA followed by Sanger sequencing of CRISPR Control, A, and B clones demonstrated gRNA target specificity within the *Rnf216/Triad3* targeted genomic regions (Figures 1B and S1A). Spectral decomposition using the Tracking of Indels by Decomposition (TIDE) tool (Brinkman et al., 2014) showed the successful creation of indels ranging from 1 to 10 base pairs for deletions and insertions (Figure S1B). Although CRISPR B lacked the presence of any wildtype (WT) *Rnf216/Triad3* sequence when compared to CRISPR control cells, CRISPR A cells contained a small fraction of WT sequence (3.1%) (Figure S1B), which agreed with our ability to detect residual full-length RNF216/TRIAD3 protein in CRISPR A cells (Figure 1A). When measuring *Gnrh* using quantitative real-time PCR (qPCR), we found a graded decrease in *Gnrh* between control, CRISPR A, and CRISPR B cells that mirrored the changes in RNF216/TRIAD3 expression. Particularly, there was a significant decrease of *Gnrh* in CRISPR B cells (p = 0.0389, One-way ANOVA; Figure 1C). Moreover, analysis of the cell culture media showed a reduction in secreted GnRH for CRISPR A (p = 0.0014) and CRISPR B cells (p = 0.0122, One-way ANOVA; Figure 1D). Considering the significant reduction of *Gnrh* in CRISPR B cells, we found that rescue of CRISPR B with wildtype CRISPR B-resistant *Rnf216/Triad3* plasmids increased *Gnrh* expression to similar levels of CRISPR control cells (Figure 1E). To determine if the activity of these cells was altered, we transfected the genetically encoded calcium indicator, R-GECO1 (Wu et al., 2013) into each CRISPR cell line (Figure 1F). We found that the event amplitudes remained similar across groups (Figure 1G), but there was a significant reduction in event frequency in CRISPR B cells compared to control cells (p = 0.0014, One-way ANOVA; Figure 1H) and CRISPR A cells (p = 0.0194). These findings suggest that loss of *Rnf216/Triad3* results in decreased *Gnrh* expression and cell activity and demonstrate that RNF216/TRIAD3 controls the production of GnRH in GnRH neuron-like cells *in vitro*.

Previously, we found that Triad3A, an abundant isoform from the *RNF216/TRIAD3* gene expressed in the brain, associates with clathrin-coated pits and alters AMPA receptor endocytosis through ubiquitination of the plasticity-associated protein, ARC (Mabb et al., 2014; Wall et al., 2018). Modulation of Triad3A also led to global changes in receptor turnover rates in primary hippocampal neurons (Figure S1C). Therefore, we attempted to measure membrane levels of the major AMPA receptor subunits, GluA1 and GluA2, in the GT1-7 cell line but were unable to detect expression for any of the groups, which is consistent with the literature that GT1-7 cells do not express these subunits (Mahesh et al., 1999). We also did not find any changes
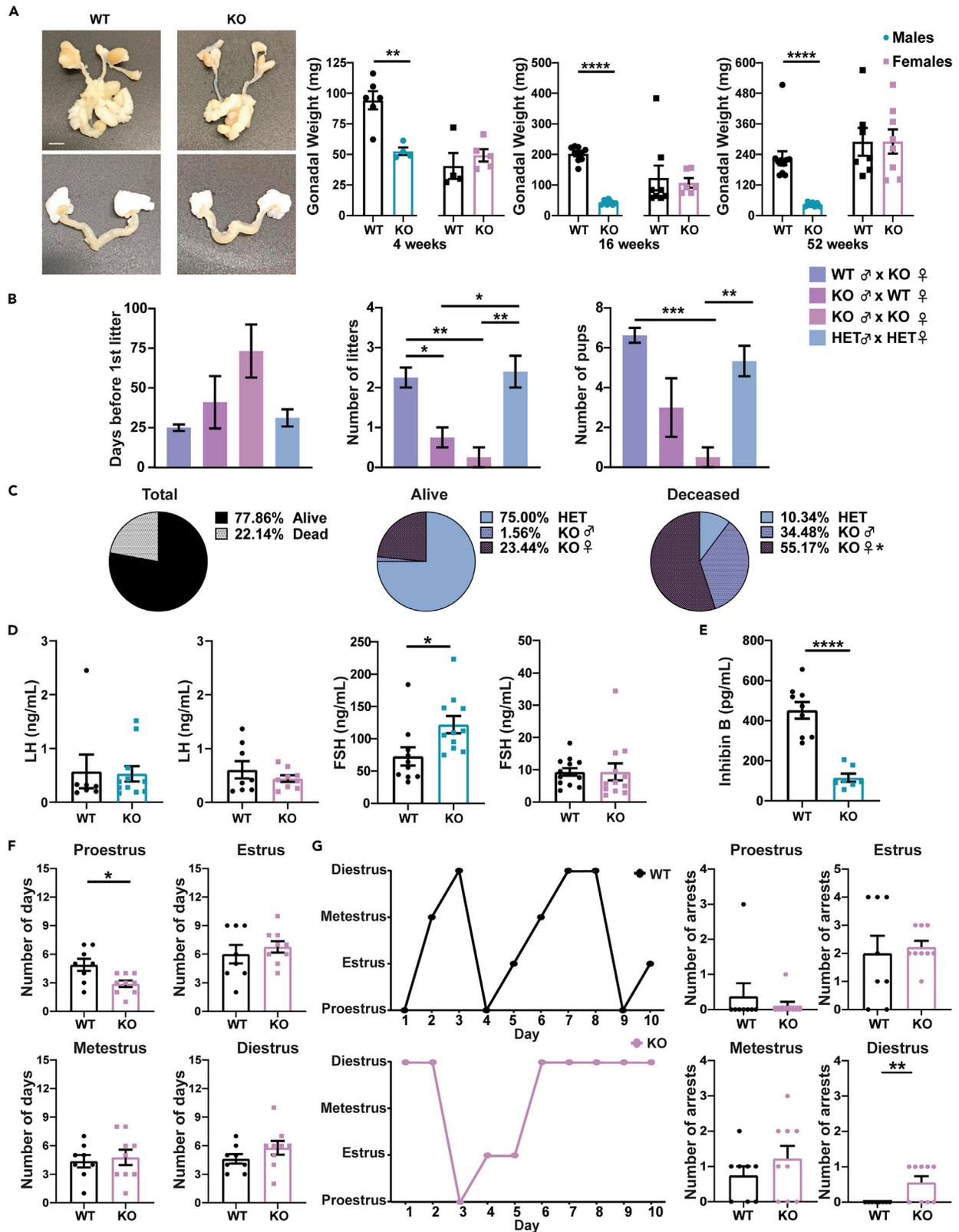
Figure 2. Male gonadal underdevelopment and reproductive deficits in *Rnf216/Triad3* knockout mice

(A) *Left*, representative images of male and female reproductive organs in WT and KO mice at 16 weeks old. Scale bar represents 25 mm. *Right*, Gonadal weights of WT and KO mice at 4-, 16-, and 52-weeks. Male KO (blue) mice show a significant reduction in testicular weights compared to WT at 4- ($t_{(8)}$ =4.321, **p = 0.0025), 16- ($t_{(13)}$ =13.96, ****p<0.0001), and 52-weeks ($t_{(17)}$ =5.065, ****p<0.0001). No significant differences in ovarian weights, which includes the fat pads surrounding the ovaries (pink). Unpaired *t*-test. N = 9–12 animals per group. Error bars are $\pm$SEM.

(B) Assessments of breeding viability in WT and KO mice at 6–7 weeks. *Left*, there were no differences in the number of days before the first litter was produced. There were significant differences in the number of litters ($F_{(3, 13)}$ =11.76, ***p = 0.0005) (*middle*) and number of pups per litter (*right*) ($F_{(3, 24)}$ = 8.213, ***p = 0.0006). One-way ANOVA with Tukey's post-hoc analysis. *p<0.05, **p<0.005, ***p<0.001, ****p<0.0001, N = 4-5 cages per genotype crossing pair and N = 8–12 pups per litter. Error bars are $\pm$SEM.

(C) Percentage of pup survival from WT and KO breeding pairs. n = 102 for pups that survived and n = 29 for pups that died. In deceased pups, KO mothers have a higher percentage compared to other genotypes ($X^2_{(2)}$ = 8.756, *p = 0.0126) Chi-square.

(D) *Left*, No differences in LH serum levels in WT and KO mice at 16-weeks. *Right*, Male KO animals have elevated FSH ($t_{(19)}$ =2.521, *p = 0.0208). No significant differences in females. N = 10–12 animals per sex per genotype. Error bars are $\pm$SEM.

(E) Male KO animals show reductions in basal inhibin B levels ($t_{(14)}$ =6.608, ****p<0.0001); Unpaired *t*-test. N = 7–10 male mice. Error bars are $\pm$SEM.

(F) Days females spent in each estrous phase for a duration of 20 days. KO females spent significantly less time in proestrus compared to WT ($t_{(15)}$ =2.809, *p = 0.0132); Unpaired *t*-test. N= 8-9 female mice per genotype. Error bars are $\pm$SEM.

(G) *Left*, Representative estrous cycle of WT and KO females. KO females showed irregular cycling compared to WT females. *Right*, Arrests in each phase of the estrous cycle of *Rnf216/Triad3* KO females for a duration of 20 days. Cycle arrests were measured as spending >1 day in proestrus, estrus, and metestrus or >2 days in diestrus. Female KO mice (Median = 1.000) significantly arrested in diestrus compared to WT (Median= 0.000). Mann-Whitney U, U= 16, *p= 0.0294. N= 8-9 female mice per genotype. Error bars are + SEM.

See also Figure S2.

in the previously identified Triad3A substrate, ARC (Figure S1D). Because GT1-7 cells express GPR54 and GnRHR (Mellon et al., 1990; Tonsfeldt et al., 2011), we reasoned that the reduction of *Gnrh* could be because of RNF216/TRIAD3-mediated trafficking of these key HPG axis receptors. We assessed changes in membrane, cytosolic, and total cell fractions of the key HPG axis receptors GPR54 and GnRHR, but found no significant differences in the membrane fractions of these receptors when normalized to total protein between groups (Figure S1E). We next measured estrogen receptor alpha (ERα), a member of the nuclear receptor family that suppresses GnRH production in the presence of estradiol (Otani et al., 2009). However, we did not find any differences in total levels of ERα (Figure S1F). The lack of changes in localization and expression of key HPG axis receptors suggest unknown mechanisms that lead to reduced *Gnrh* and Ca^{2+} transients in GT1-7 cells.

Generation of *Rnf216/Triad3* KO mice

We next sought to evaluate the role of *Rnf216/Triad3* within an intact HPG axis by generating a constitutive *Rnf216/Triad3* knockout (KO) mouse. *Rnf216/Triad3*$^{fl/fl}$ mice were crossed with the female homozygous CMV-CRE global deleter line (*CMV-X*^{CRE}*X*^{CRE}) (Schwenk et al., 1995) and the CRE was bred out to avoid phenotypic effects (Figure S2A). Genotypes of mice were validated (Figure S2B) and corresponding representative immunoblots demonstrated a significant loss of RNF216/TRIAD3 in the hypothalamus and gonads of KO mice (Figure S2C). Although there was a significant decrease in body weight in 4-week-old male KO mice, we found no significant difference in body weights in male and female KO mice up to 52 weeks old (Figure S2D). Normalized brain weights also showed a main effect of sex in 16- (p< 0.0001) and 52-week-old mice (p = 0.0004 two-way ANOVA; Figure S2E), but there were no genotypic differences. Similar to our findings in *Rnf216/Triad3* KO GT1-7 cells (Figures S1D–S1F), there were no differences in expression of GPR54, GnRHR, ERα, or ARC in the hypothalamus of KO mice from both sexes (Figure S2F).

Constitutive *Rnf216/Triad3* KO mice have reproductive impairments

As stated previously, individuals with GHS display HH and reproductive impairments. Upon further inspection of the reproductive organs, we found that male KO animals had dramatically reduced testicular weights compared to WT at 4- (p = 0.0025, unpaired *t*-test; Figure 2A), 16- (p< 0.0001), and 52-week (p< 0.0001). This was not evident in ovaries isolated from KO females. We next determined if the altered testicular weight in males affected breeding viability. We paired WT male:KO female, KO male:WT female, KO male:KO female, and HET male:HET female mice for a maximum of 90 days (Figure 2B). In all pairings, there were no significant differences in the number of days before the first litter, indicating all genotypes could produce litters (Figure 2B, left). Nevertheless, there were significant differences in the number of litters produced by each cage (p = 0.0005, One-way ANOVA; Figure 2B, middle). WT male:KO Female pairings had significantly more litters than KO male:WT female (p = 0.0270) and KO male:KO female (p = 0.0037) pairings. HET male:HET female pairings had significantly more litters than KO male:WT female (p = 0.0104) and

KO male:KO female (p = 0.0013) pairings. There were no differences between HET male:HET female and WT male:KO female pairings. Within litters, we also observed a significant difference in the total number of pups across all litters (p = 0.0006, One-way ANOVA; Figure 2B, right). KO male:KO female pairings produced a significantly lower number of pups than WT male:KO female (p = 0.0006) and HET male:HET female pairings (p = 0.004). Notably, some litters did not survive past P7; therefore, we assessed pup survival (Figure 2C). Out of the 77.86% of pups that survived, only 1.56% originated from KO male breeders and 23.44% from KO female breeders who successfully grew to weaning age at P21. Surprisingly, of the 22.14% of pups that did not survive, 34.48% of pups came from KO male breeders and 55.17% of pups came from KO female breeders (p = 0.0126, Chi-square), suggesting that there is a failure of pups to thrive with KO female mothers within the first week of postpartum.

Because of these alterations in breeding, we also determined if there was an associated change in HPG axis hormones that could explain the reductions in testicular weight in male KO mice and a failure of pups to thrive with female KO mothers. Blood sera levels of the pituitary hormones FSH and LH were measured in males and females at 16 weeks old. Surprisingly, neither males nor females exhibited alterations in baseline LH (Figure 2D, left). Despite no differences in FSH between WT and KO females, KO males had a significant increase in circulating FSH (p = 0.0208, unpaired t-test; Figure 2D, right) compared to WT males. One explanation for elevated FSH in males, without alterations in LH, could be because of impairments in gonadal feedback loops. One such peptide hormone that negatively regulates FSH in males is inhibin B, which is produced by Sertoli cells in the testes (Luisi et al., 2005). Indeed, we found that KO males had significant reductions in inhibin B compared to WT (p< 0.0001, unpaired t-test; Figure 2E), suggesting a causative role for increased FSH because of downregulated inhibin B. Although there were no hormonal changes between WT and KO females, when evaluating the estrous cycle for 20 days, KO females spent significantly less time in proestrus (p = 0.0132, unpaired t-test, Figure 2F). Moreover, WT females cycled regularly throughout the different estrous phases whereas KO females had abnormal cycling patterns (Figure 2G) with frequent cycle arrests in the diestrus phase (p = 0.0294, Mann-Whitney U). These findings suggest that in females, hormonal surges that control the transition of the estrous phases (proestrus to estrus) are likely to be disordered.

Constitutive *Rnf216/Triad3* KO mice have altered GnRH morphology

In view of *Rnf216/Triad3* KO mice displaying sex differences in reproductive impairment and the variability of GHS patient responses to exogenous GnRH treatment (Margolin et al., 2013; Seminara et al., 2002), we determined if GnRH neurons within the HPG axis were altered *in vivo*. GnRH neurons undergo a migratory and maturation process from the nasal placode to the hypothalamus during embryonic and postnatal development (Cottrell et al., 2006; Jasoni et al., 2009). A recent study using GN11 cells, an immature GnRH neuronal cell line, suggested that migration of GnRH neurons to the hypothalamus could be reduced upon depletion of RNF216/TRIAD3 (Li et al., 2019). Thus, we evaluated if GnRH cell density and morphologies were disrupted within the preoptic area of the hypothalamus in adult KO mice. Histological analysis of the preoptic area of the hypothalamus in male and female KO mice showed no significant differences in the density of GnRH neurons or the number of dendrites protruding off the soma (Figures 3A and S3A). We next categorized GnRH neurons by dendritic morphologies based on their number of dendrites which reflects their maturity. In the hypothalamus, mature GnRH neurons are characterized as having unipolar and bipolar dendritic morphologies whereas immature GnRH neurons contain multiple branches (>2) (Cottrell et al., 2006). We classified GnRH cells as none (zero dendrites), unipolar (1 dendrite), bipolar (2 dendrites), and multipolar (>2 dendrites) (Figure S3B) as previously described (Tata et al., 2017). Although KO mice exhibited a higher percentage of none type GnRH neurons (12.78% in males and 16.07% in females) compared to WT (8.11% in males and 7.97% in females), there were no significant differences as assessed by a Chi-square analysis (Figure 3B). On the contrary, we found a difference in the soma size of GnRH neurons, which was significantly reduced in KO males (p = 0.0025, unpaired t-test; Figure 3C, left) and KO females (p = 0.0202; Figure 3C, right). Moreover, there was a significant decrease in the integrated density of GnRH in KO males (p = 0.0111, unpaired t-test; Figure 3C) and KO females (p = 0.0447) indicating that they may contain less GnRH, which aligned with our *in vitro* data (Figures 1C and 1D).

Constitutive *Rnf216/Triad3* KO mice have altered microglia

RNF216/TRIAD3 participates in innate inflammatory signaling pathways (Chuang and Ulevitch, 2004; Fearns et al., 2006; Nakhaei et al., 2009) and individuals with GHS were found to have increased gliosis (Alqwaifly and Bohlega, 2016; Calandra et al., 2019; Margolin et al., 2013; Mehmood et al., 2017). Notably,
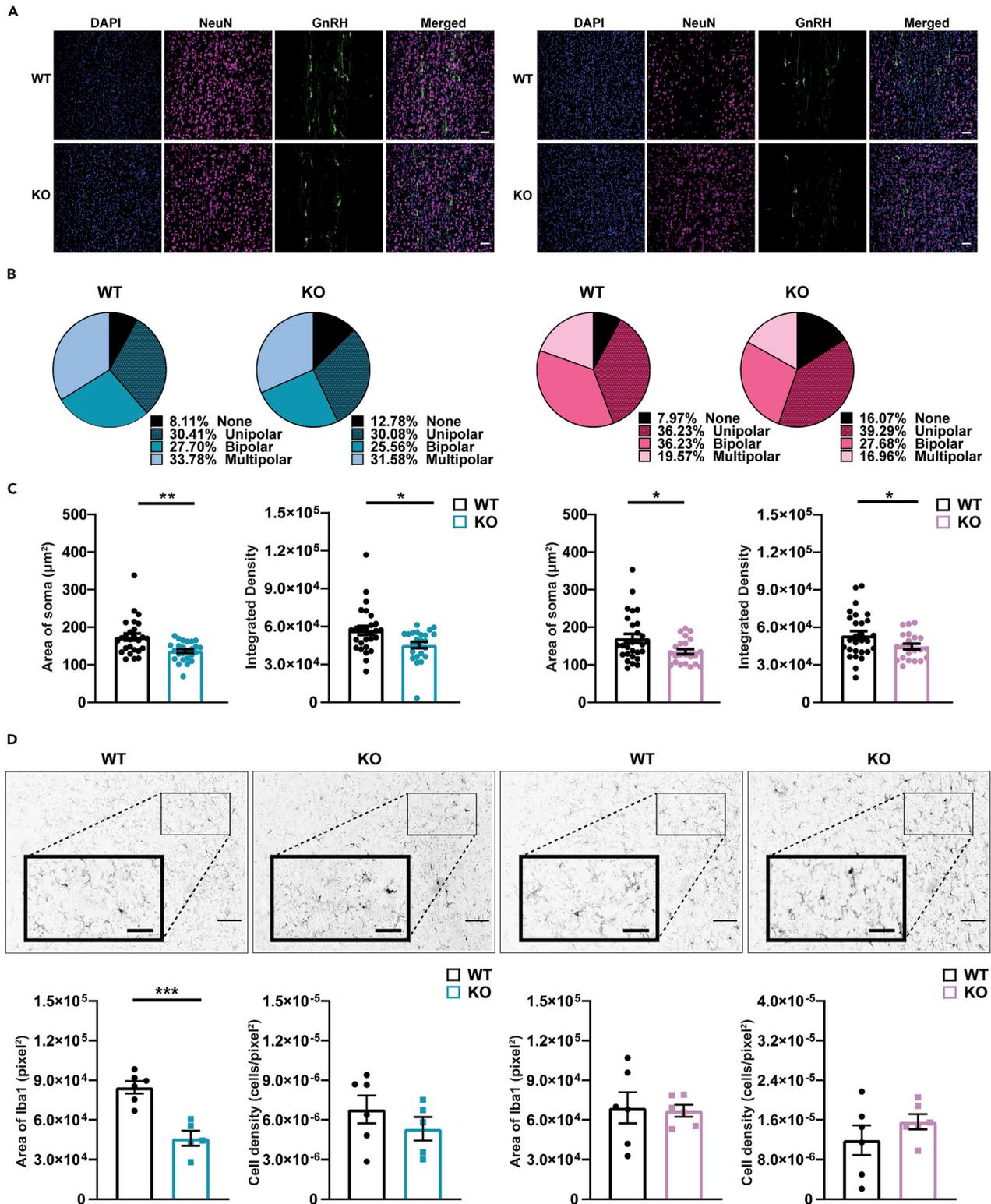
Figure 3. Loss of RNF216/TRIAD3 decreases GnRH soma size and GnRH production in both sexes and increases neuroinflammation in males

(A) Representative confocal images of GnRH cells in the preoptic area of the hypothalamus in adult WT and KO male (*left*) and female (*right*) mice. GnRH neurons were imaged at 20× magnification. Scale bars represent 50 μm.

Figure 3. *Continued*

(B) GnRH neurons were classified according to the number of dendrites protruding directly off the soma: none (zero dendrites), unipolar (1 dendrite), bipolar (2 dendrites), multipolar (>2 dendrites). Although KO animals had a higher percentage of none type compared to WT, this was not significantly different in males (X^2(3) = 1.709, p = 0.6349) or females (X^2(3) = 5.198, p = 0.1579). Chi-square. For males per genotype, n= 12–17 cells for none, n= 40–45 cells for unipolar, n= 34–41 cells for bipolar, and n= 42–50 cells for multipolar. For females per genotype, n= 11–18 cells for none, n= 44–50 cells for unipolar, n= 31–50 cells for bipolar, and n= 19–27 cells for multipolar.

(C) Significant differences in soma area in males (t (50) =3.185, **p=0.0025) and females (t (48) =2.402, *p = 0.0202) compared to respective WT counterparts. There were also significant differences in the integrated density in KO males (t (50) =2.637, *p = 0.0111) and females (t (48) =2.061, *p = 0.0447) compared to respective WT; Unpaired t-test. N = 3 for males per genotype with 4–6 sections per animal represented in summary plots. N = 3 for females per genotype with across 3–4 sections per animal represented in summary plots. Error bars are ±SEM.

(D) *Top*, representative images of microglia stained with Iba1 in the preoptic area of the hypothalamus in WT and KO males (left) and females (right) were imaged at 10x magnification. Scale bars represent 100 μm. *Bottom*, KO males show lower Iba1 total area (including processes) compared to WT (t (9) =5.280, ***p = 0.0005; Unpaired t-test). N = 3 for males per genotype with one to two sections per animal represented in summary plots. No significant differences in females. N = 3 for females per genotype with two sections per animal represented in summary plots. No significant differences in cell density. Error bars are ±SEM.

See also Figure S3.

inflammatory pathway constituents have been demonstrated to control GnRH production and release (Lainez and Coss, 2019; Zhang et al., 2013). To determine if the loss of RNF216/TRIAD3 leads to neuroinflammation, we analyzed astrocytes and microglia in the preoptic area of the hypothalamus. We found no significant differences in astrocyte density in male and female KO mice (Figure S3C). However, male (p = 0.0005, unpaired t-test; Figure 3D), but not female KO mice, showed a significant reduction in microglia total area but not cell density. To determine if the changes in microglial morphology were related to a neuroinflammatory environment, we measured changes in proinflammatory cytokines in the hypothalamus. Although we did not observe a change in *Tnfa* in either sex (Figure S3D), there was a selective increase in *Il1b* in male KO mice (Figure S3E), suggesting increased neuroinflammation in this region.

Generation of central nervous system-specific *Rnf216/Triad3* KO mice

Given the broad distribution of RNF216/TRIAD3 in and out of the nervous system, we sought to spatially control the expression of RNF216/TRIAD3 via selective deletion in neural stem cell/precursor cells. We bred *Rnf216/Triad3^{fl/fl}* conditional mice with the *Nestin*-CRE mouse line (Tronche et al., 1999; Zimmerman et al., 1994). Representative immunoblots demonstrated a significant loss of RNF216/TRIAD3 in the brain, but not in the gonads (Figure S4A). Similar to *Rnf216/Triad3^{−/−}* constitutive KO mice, there were no differences in brain (Figure S4B) or body weights (Figure S4C).

Unlike *Rnf216/Triad3^{−/−}* constitutive KOs, *Nestin*-CRE:*Rnf216/Triad3^{fl/fl}* male KO mice did not show reductions in gonadal weights at 16- and 52-weeks compared to WT males (Figure 4A) or changes in breeding viability (data not shown). Moreover, there were no genotypic differences in FSH levels in male KO mice (Figure 4B) or changes in female estrous cycles (Figures S4D and S4E). We also analyzed GnRH expression and cell morphologies but did not find any genotypic differences in males or females (Figures 4C–4E), except that female KO mice showed an increase in cell density (p =0.0234, unpaired t-test; Figure S4F). Cumulatively, these findings indicate that central nervous system (CNS)-specific deletion of *Rnf216/Triad3* does not cause HPG axis impairments. In addition to the lack of HPG axis effects, we also found that CNS-specific KO mice had no differences in GFAP cell density (Figure S4G). Although, adult KO males did have reduced microglia area (p = 0.005, unpaired t-test; Figure 4F) that was also accompanied by a decrease in cell density (p = 0.0267). There were no differences found in females. Thus, CNS-specific KO male mice have abnormal microglial expression, which appears to be independent of HPG axis disruption.

DISCUSSION

RNF216/TRIAD3 is an E3 ligase that ubiquitinates substrates involved in inflammation and immunity (Chuang and Ulevitch, 2004; Fearns et al., 2006; Nakhaei et al., 2009), autophagy (Kim et al., 2018; Wang et al., 2016; Xu et al., 2014), and synaptic plasticity (Mabb et al., 2014; Wall et al., 2018). Although mutations in *RNF216/TRIAD3* cause GHS, the role of RNF216/TRIAD3 within the HPG axis has not been elucidated. Here, we found that constitutive deletion of *Rnf216/Triad3* results in reproductive impairment at multiple levels within the HPG axis, uniquely affecting males and females. Loss of *Rnf216/Triad3* leads to abnormal GnRH production, activity, and neuronal size in both males and females; yet, only KO males showed changes in FSH, gonadal development, and breeding viability. Activated microglia were also identified in adult KO males but not in KO females. Instead, KO females
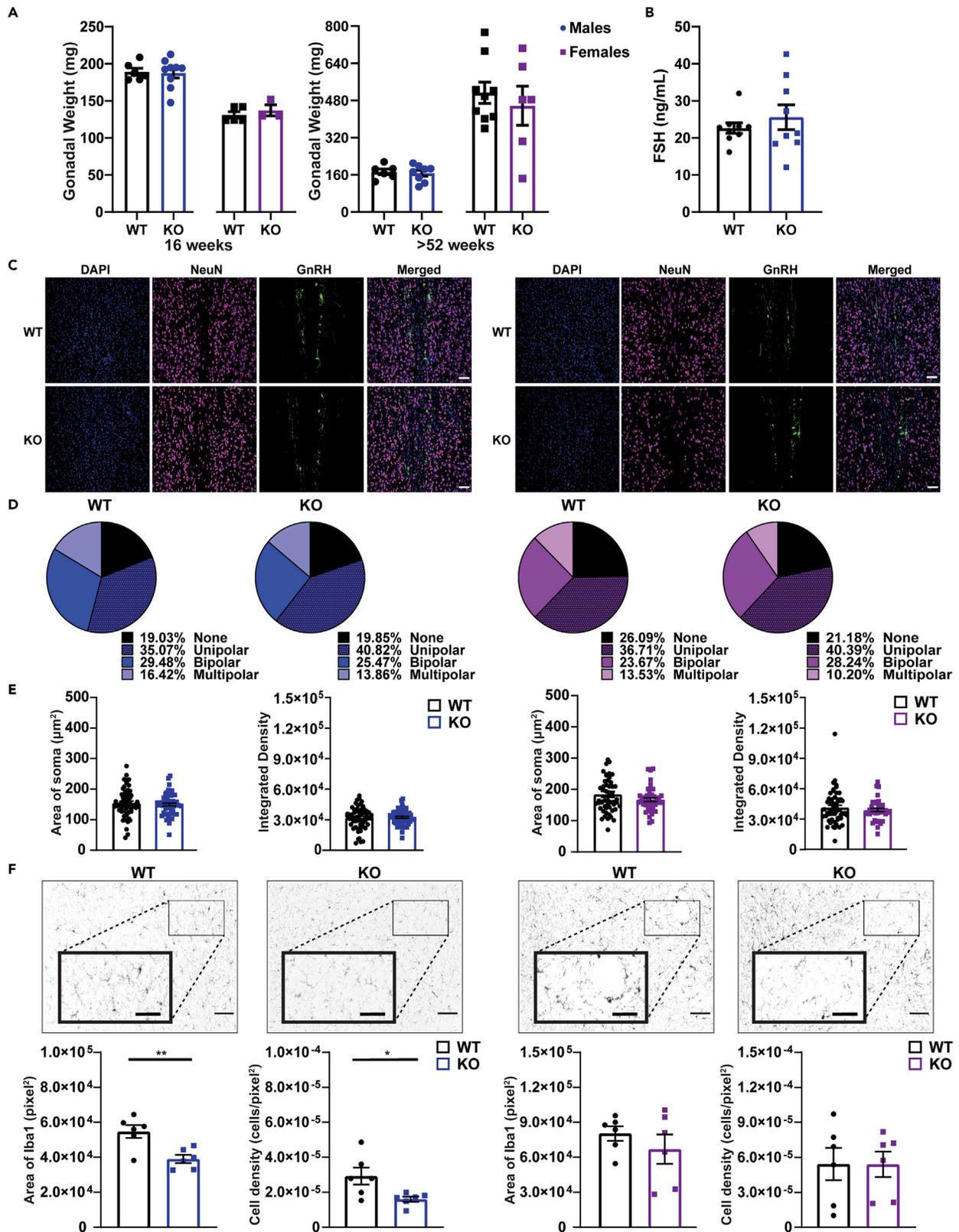
Figure 4. *Rnf216/Triad3* CNS-specific knockout mice do not demonstrate reproductive deficits but KO males have altered microglia

(A) Gonadal weights of *Rnf216/Triad3* Nestin-CRE WT and KO mice at 16-, and 52-weeks. There were no significant differences at either age. N = 3–10 animals per genotype.

(B) There were no significant differences in FSH levels in *Rnf216/Triad3* Nestin-CRE KO male animals. N = 9–10 animals per genotype.

(C) Representative confocal images of GnRH cells in the preoptic area of the hypothalamus in adult *Rnf216/Triad3* Nestin-CRE WT and KO male (*left*) and female (*right*) mice. GnRH neurons were imaged at 20× magnification. Scale bars represent 50 μm.

(D) GnRH neurons were classified according to the number of dendrites protruding directly off the soma. There were no significant differences between WT and KO in males or females. For males per genotype, n= 51–53 cells for none, n= 94–109 cells for unipolar, n= 68–79 cells for bipolar, and n= 37–44 cells for multipolar. For females per genotype, n= 54 cells for none, n= 76–103 cells for unipolar, n= 49–72 cells for bipolar, and n= 26–28 cells for multipolar.

(E) There were no significant differences in the area of the soma or integrated density in *Rnf216/Triad3* Nestin-CRE KO males or females. N = 3 for males with seven to eight sections per animal represented in summary plots. N = 3 for females with six to eight sections per animal represented in summary plots.

(F) *Top*, representative images of microglia stained with Iba1 in the preoptic area of the hypothalamus in *Rnf216/Triad3* Nestin-CRE WT and KO males (left) and females (right) imaged at 10x magnification. Scale bars represent 100 μm. *Bottom*, there were significant differences in Iba1 area (including processes) in males (t (10) =3.584, **p = 0.005; Unpaired t-test). There were significant differences in cell density in males (t (10) =2.595, *p = 0.0267; Unpaired t-test). N = 3 for males per genotype with two sections per animal represented in summary plots. No differences in females. N = 3 for females per genotype with two sections per animal represented in summary plots. Error bars are ±SEM.

See also Figure S4.

had estrous cycle abnormalities, with decreased time spent in proestrus and increased cycle arrests in the diestrus phase.

Because of the role of TRIAD3A in the CNS, we sought to determine if the loss of RNF216/TRIAD3 affected GnRH neuron activity and secretion. Using the CRISPR-Cas9 system in a GnRH hypothalamic-derived cell line (GT1-7), we generated two *Rnf216/Triad3* KO cell lines. *Gnrh* and baseline calcium frequency were significantly reduced following KO, suggesting that a decrease in the activity of these cells leads to inefficient GnRH release. The cell-autonomous feature of RNF216/TRIAD3 paralleled our *in vivo* constitutive knockout data illustrating abnormal GnRH expression and decreased GnRH soma size. However, we did not observe any neuroendocrine phenotypes after crossing conditional *Rnf216/Triad3* mice with the *Nestin*-CRE line, which leads to selective deletion of *Rnf216/Triad3* in neural stem cell precursors. Our findings show that CNS-specific removal of *Rnf216/Triad3* is not sufficient to cause dysfunctional HPG axis phenotypes and that RNF216/TRIAD3 most likely plays a prominent role in HPG axis dysfunction at the level of the pituitary and/or gonads. These findings also indicate that complete removal of RNF216/TRIAD3 is required for achieving a phenotypic effect and is consistent with the recessive nature of inheritance for GHS (Alqwaifly and Bohlega, 2016; Margolin et al., 2013).

Disease-causing mutations of *RNF216/TRIAD3* are known to decrease its E3 enzymatic activity and disrupt ARC ubiquitination, providing strong evidence that ubiquitination of substrates is a major contributing factor for GHS (Husain et al., 2017; Mabb et al., 2014). However, we did not find evidence of changes in ARC in GT1-7 KO cells or the hypothalamus of *Rnf216/Triad3* KO mice. Moreover, a transgenic mouse that contains mutations in RNF216/TRIAD3 ARC ubiquitination sites did not cause reproductive impairments (Wall et al., 2018), inferring RNF216/TRIAD3-dependent regulation of other substrates regulate HPG axis functions. TRIAD3A can ubiquitinate ARC, which stimulates AMPA receptor trafficking in the hippocampus (Mabb et al., 2014), and we found that knockdown of TRIAD3A decreased receptor trafficking. Therefore, we determined if RNF216/TRIAD3 could alter membrane localization of GPR54, a kisspeptin receptor found in GnRH cells that precedes the release of GnRH. However, we found no differences in membrane localization of GPR54 and GnRHR in *Rnf216/Triad3* GT1-7 KO cells nor did we observe changes in GPR54, GnRHR, and ERα at steady-state both *in vitro* and *in vivo*. Given our inability to identify targets, then, what could be potential RNF216/TRIAD3 substrates in GnRH neurons?

Although we did not find changes in GPR54 or GnRHR expression, the altered calcium signaling we observed suggests that there are other intrinsic factors that RNF216/TRIAD3 interacts with to affect baseline calcium responses. Depolarization of GnRH neurons activates the phospholipase C-β signaling pathway that engages transient receptor potential channels (Rønnekleiv and Kelly, 2013; Zhang et al., 2008). GnRH transcription and secretion are increased through hydrolysis of phosphatidylinositol 4,5-bisphosphate, which leads to Ca^{2+} mobilization and activation of protein kinase C (Wetsel et al., 1993; Wetsel and Negro-Vilar, 1989). GnRH release is also affected by voltage-gated Ca^{2+} channels that include L-type and T-type channels that modulate burst firing in GnRH neurons through estradiol stimulation (Lee et al., 2010; Watanabe et al., 2004; Zhang et al., 2009) as well as Ca^{2+}-dependent chloride channels in different

model systems, including GT1-7 cells (Weyler et al., 1999; Yoshida et al., 1989). It is therefore possible that RNF216/TRIAD3 may ubiquitinate these factors to regulate GnRH neuron activity.

Another factor involved in signaling leading to the production of GnRH is nuclear factor kappa-light-chain-enhancer of activated B cells (NF-κB) (Zhang et al., 2013). RNF216/TRIAD3 ubiquitinates multiple proteins within the innate immunity pathway, which alter NF-κB activity (Alturki et al., 2018; Chuang and Ulevitch, 2004; Fearns et al., 2006; Nakhaei et al., 2009). Interestingly, both NF-κB and inhibitor of nuclear factor kappa B kinase subunit beta (IKK-β) activation reduce GnRH release from GT1-7 cells (Zhang et al., 2013). Inducing neuroinflammation via lipopolysaccharide injection in male mice also resulted in a decrease in *Gnrh1* (Lainez and Coss, 2019). Given that RNF216/TRIAD3 is ubiquitously expressed in and outside the nervous system and its role in regulating NF-κB, we speculated that its removal would create a neuroinflammatory environment that would result in reduced GnRH secretion in males and females. However, when surveying the resident microglia immune cells in the preoptic area of hypothalamus, only *Rnf216/Triad3* KO males had increased *Il1b* and reduced microglia cell area (suggestive of less ramified microglia and indicative of activated microglia). Therefore, our findings do not adequately support a role for microglia in regulating GnRH neurons in this region. One major cell type that controls GnRH activity is astrocytes (Pellegrino et al., 2021; Sharif et al., 2013); however, we found no change in astrocyte density or area in male and female KOs. One aspect to consider from our data is that the progression of neuroinflammation may differ between male and female GHS patients. These findings are not overly surprising given the numerous studies demonstrating female resilience to neuroinflammation in other rodent models for neurodegenerative disease (Hanamsagar et al., 2017; Schwarz et al., 2012). The added protection in females may be because of the expression of specific gonadal hormones such as estradiol, which induces prostaglandin E_2 (PGE_2) (Lenz et al., 2013), and exposure to estrogens, which are suggested to reduce the neuroinflammatory environment (Vegeto et al., 2001). RNF216/TRIAD3 may also be required for the transition of inflammatory microglia to their quiescent ramified state in males, which is signaled by an androgen surge in the testes and is critical for masculinizing the brain (Vegeto et al., 2001). Future directions would be aimed at conducting a longitudinal study in male and female KO mice to determine if females would eventually develop neuroinflammation in this region. Moreover, GHS patients also exhibit neurodegeneration in multiple brain regions (e.g. cerebellum, cortex, hippocampus, and brain stem) (Alqwaifly and Bohlega, 2016; Calandra et al., 2019; Lieto et al., 2019; Margolin et al., 2013; Mehmood et al., 2017) so these areas should also be characterized thoroughly.

As we moved downstream within the HPG axis, we found that deletion of *Rnf216/Triad3* led to sex-specific gonadotropin hormone release and reproductive function. KO males exhibited decreased testicular weight and reduced breeding viability similar to findings in another *Rnf216/Triad3* KO mouse (Melnick et al., 2019) and a recent study that generated a separate *Rnf216/Triad3* KO mouse using CRISPR-Cas9 (Li et al., 2021). Male fertility was completely abolished in both of these studies as measured by paired matings. However, neither study provided a combination of important details for breeding regarding the age of pairing and the duration of these pairings. It is important to note that the amount of sperm from 8-week-old mice was dramatically reduced but not completely eradicated in the Li et al. KO mouse. In our study, we paired mice during their peak of breeding (6–8 weeks) for a duration of 90 days, primed the female cages with male bedding, and singly housed male cages with female bedding 48 h before pairing. Importantly, we counted all pups on Day 0 after they were born, as pups can die or be cannibalized by their parents prior to weaning. Using optimal breeding conditions, we found a dramatic reduction in the number of litters and the number of pups produced with KO males, which is consistent with the reduced spermatogenesis observed in these two studies. Since the other two studies did not specify their breeding conditions and which time point they counted pups, we cannot conclude the exact reason for these discrepancies. Although we did not look at spermatogenesis, we believe that is also impaired in our mouse model since we observed significantly reduced litter sizes in WT females that have been mated with KO males. Additionally, these KO males have reduced inhibin B, which is generated by Sertoli cells in the testes to promote spermatogenesis (Meachem et al., 2001). Although KO females did not show a reduction in ovarian weights, they displayed irregular estrous cycling, with more frequent arrests in diestrus and decreased time spent in proestrus, the phase essential for successful reproduction.

KO male mice displayed elevated FSH without changes in LH, whereas females did not show differences in the release of these pituitary hormones at the same time point. GnRH regulation of FSH and LH release occur via distinct mechanisms from the anterior pituitary (Kile and Nett, 1994). Male gonadotropes have

been suggested to respond differently because of subtle changes in GnRH neuron activity and GnRH production via feedback regulation (Tilbrook and Clarke, 2001). Sex differences in FSH release may also arise from sexual dimorphism in gonadotropes themselves. For example, although expressed in both male and female gonadotropes, FSH selectively colocalizes with the neuronal Ca^{2+} sensor synaptotagmin-9 (syt-9) in females to facilitate FSH exocytosis. Deletion of *syt-9* in mice decreases basal and stimulated FSH secretion exclusively in females and alters their estrous cycle, without any effect on males (Roper et al., 2015). Additional sex-specific molecular factors may govern FSH release in males, for which RNF216/TRIAD3 may be a likely candidate. Inhibin A and B are glycoproteins that also control the synthesis and release of FSH secreted in a sex-dependent way (Groome et al., 1996; Kubini et al., 2000; Luisi et al., 2005; Welt et al., 1997) and clinically, men with HH display low levels of inhibin B (Coutant et al., 2010). With the reduction of testicular weight in the KO males, we hypothesized that this results in decreased inhibin B release from Sertoli cells to reduce FSH synthesis and release. Indeed, we found that male KO mice had significantly lower levels of inhibin B indicating that the elevation of FSH was likely caused by the loss of this negative feedback loop.

Our results regarding differences in males and females in reproductive function may be in alignment with GHS individuals. Likely, individual point mutations within regions of the *RNF216/TRIAD3* gene create broad phenotypes of HH while also displaying nuances in reproductive impairment. For example, male patients with mutations in the c.2061G>A location demonstrate poor development of secondary sexual characteristics, hypogenitalism, gynecomastia, and low testosterone with no changes in FSH (Alqwaifly and Bohlega, 2016). Males with compound heterozygous mutations in the E205fsX15 + C597X region were diagnosed with HH with low testosterone concentration in adulthood (Margolin et al., 2013; Mehmood et al., 2017). In contrast, a female patient with an R751C mutation found within the E3 ligase catalytic domain had menarche at 16 years old followed by secondary amenorrhea whereas another female patient with a p.G138GfsX74 mutation, had oligomenorrhea followed by amenorrhea at 27 years old (Margolin et al., 2013). Although one female patient that was heterozygous for one intronic (c.2061+3A>G) and one missense (c.1849A>G;p.M617V) mutation presented with slightly subnormal FSH and LH levels. She also had normal levels of progesterone and estradiol along with two successful pregnancies (Lieto et al., 2019). Based on this clinical literature and findings from our KO mouse, we conclude that mutations in *RNF216/TRIAD3* result in less drastic neuroendocrine phenotypes in females compared to males which may further be confounded by the location of *RNF216/TRIAD3* mutations.

We acknowledge that gonadal failure in males could be the sole cause of male reproductive dysfunction. It is important to mention that Li et al. found that the Sertoli cells were normal in the testes of *Rnf216/Triad3* KO mice (Li et al., 2021), which is in stark contrast to Melnick et al. that observed testicular germ cell degeneration (Melnick et al., 2019). We tried to resolve these discrepancies by assessing reproductive and hormonal phenotypes in *Rnf216/Triad3* conditional KO mice. One surprising aspect of our study was our findings related to neural stem cell-specific knockout of *Rnf216/Triad3*. Here, CNS-specific deletion of *Rnf216/Triad3* resulted in no differences in gonadal weights in males. This lack of phenotype was also consistent with no change in FSH, GnRH neuron size, or GnRH expression. This is fundamental as there is controversy in the literature regarding elevated FSH in the control of male gonadal size (Plant and Marshall, 2001; Santi et al., 2020). Our data support the relationship between elevated FSH and reduced testicular size found in our male constitutive KO mouse. These findings also suggest that peripheral actions of RNF216/TRIAD3 may be the main cause of HH in males, most likely at the level of the pituitary and/or gonads to disrupt neuroendocrine function. Based on these results, we hypothesize that HPG axis dysfunction in GHS is mainly caused by gonadal failure, resulting in defective feedback loops that drive GnRH neural function and morphology. Since our CNS-specific knockout could not recapitulate the same phenotypes demonstrated in our constitutive knockout, this indicates that selectively deleting *Rnf216/Triad3* in the brain does not regulate basal hypothalamic neuroendocrine activity. Although peripheral actions of GHS led to HPG axis dysfunction, removal of RNF216/TRIAD3 in the CNS still resulted in an inability to regulate microglia 'states' in males. Given that microglia are generated from macrophages and not neural stem cells (Ransohoff and Perry, 2009), RNF216/TRIAD3 should still be present in these cell types within the preoptic area. These findings suggest that CNS-specific actions of RNF216/TRIAD3 are somehow important for maintaining a healthy male microglia environment, which may be a factor that increases susceptibility to neurodegeneration in GHS patients.

Conclusion

Our findings suggest that the effects of RNF216/TRIAD3 loss disrupt multiple points within the HPG axis with an additional role in neuroinflammation. Our work highlights the importance of ubiquitination in proper HPG axis function. By establishing its pathophysiology, it may be possible to identify sex-specific targets for GHS and other neuroendocrine disorders related to ubiquitin disruption.

Limitations of the study

Our findings pose an important advancement in the field that describes distinct functions of E3 ubiquitin ligases in neuroendocrine function in males and females and provides new insight into therapeutics for Gordon Holmes syndrome (GHS) that are peripherally and centrally targeted. One limitation of this work is an inability to identify a potential mechanism leading to the downregulation of GnRH and its secretion. We have been actively pursuing alterations in established mechanisms with limited success. These findings hint at an unidentified pathway that regulates GnRH transcription and/or secretion, which we address in the Discussion. Overall, our results do indicate that reduced *GnRH* transcription is likely due to a loss of RNF216, as the expression of CRISPR-resistant mouse RNF216 isoforms A and B could restore *GnRH*. Finally, the sample size for immunohistochemical characterization of GnRH neurons, astrocytes, and microglia are within range of previously published studies, but may be perceived as small by some researchers. We used a total of three animals per genotype and multiple stereologically matched sections per animal. These data are displayed from individual sections in the summary figure plots.

STAR★METHODS

Detailed methods are provided in the online version of this paper and include the following:

- KEY RESOURCES TABLE
- RESOURCE AVAILABILITY
  - Lead contact
  - Materials availability
  - Data and code availability
- EXPERIMENTAL MODEL AND SUBJECT DETAILS
  - Animals
  - Generation of Rnf216/Triad3 knockout mice
  - Generation of Nestin-CRE::Rnf216/Triad3 Mice
  - Cloning of control and Rnf216/Triad3 CRISPRs
  - Cell culture and generation of control and Rnf216/Triad3 CRISPR clones
  - Validation of CRISPR sequences
- METHOD DETAILS
  - Blood collection and ELISA
  - Vaginal cytology
  - Breeding viability
  - Immunohistochemistry
  - Iba1 and Gfap staining and imaging
  - RT-qPCR
  - GnRH ELISA
  - GT1-7 CRISPR rescue
  - Subcellular fractionation
  - Western blotting
  - Transferrin receptor uptake in neurons
  - Calcium imaging
- QUANTIFICATION AND STATISTICAL ANALYSIS

SUPPLEMENTAL INFORMATION

Supplemental information can be found online at https://doi.org/10.1016/j.isci.2022.104386.

AUTHOR CONTRIBUTIONS

A.J.G. conceived and performed almost all the experiments including generation and maintenance of GT1-7 CRISPR clones and *Rnf216/Triad3* mice, conducted the data acquisition and analysis, and wrote and edited the manuscript. C.W. cloned *Rnf216/Triad3* CRISPR plasmids. Y.C.H. cloned *Rnf216/Triad3* CRISPR plasmids and edited the manuscript. B.D. and N.F. provided instrumentation, performed the calcium imaging, and edited the manuscript. H.L. performed the ELISA experiment and analysis. M.G. stained and imaged Iba1 and GFAP sections and analyzed the Iba1 sections. E.H. provided the GnRH antibody. A.Z.M., D.W., and E.H. edited the manuscript. A.M.M. conceived the experiments, generated the *Rnf216/Triad3* mouse colony, performed the transferrin receptor trafficking experiment, collected blood samples for hormonal analysis and brains for histological analysis, wrote and edited the manuscript, and supervised the study.

DECLARATION OF INTERESTS

The authors declare no competing interests.

INCLUSION AND DIVERSITY

We worked to ensure sex balance in the selection of non-human subjects. One or more of the authors of this paper self-identifies as an underrepresented ethnic minority in science.

REFERENCES

Achrekar, S.K., Modi, D.N., Meherji, P.K., Patel, Z.M., and Mahale, S.D. (2010). Follicle stimulating hormone receptor gene variants in women with primary and secondary amenorrhea. J. Assist. Reprod. Genet. *27*, 317–326. https://doi.org/10.1007/s10815-010-9404-9.

Alqwaifly, M., and Bohlega, S. (2016). Ataxia and hypogonadotropic hypogonadism with intrafamilial variability caused by RNF216 mutation. Neurol. Int. *8*, 6444. https://doi.org/10.4081/ni.2016.6444.

Alsemari, A. (2013). Hypogonadism and neurological diseases. Neurol. Sci. *34*, 629–638. https://doi.org/10.1007/s10072-012-1278-4.

Alturki, N.A., McComb, S., Ariana, A., Rijal, D., Korneluk, R.G., Sun, S.-C., Alnemri, E., and Sad, S. (2018). Triad3a induces the degradation of early necrosome to limit RipK1-dependent cytokine production and necroptosis. Cell Death Dis. *9*, 592. https://doi.org/10.1038/s41419-018-0672-0.

Angulo, M.A., Butler, M.G., and Cataletto, M.E. (2015). Prader-Willi syndrome: a review of clinical, genetic, and endocrine findings. J. Endocrinol. Invest. *38*, 1249–1263. https://doi.org/10.1007/s40618-015-0312-9.

Armstrong, S.P., Caunt, C.J., Fowkes, R.C., Tsaneva-Atanasova, K., and McArdle, C.A. (2009). Pulsatile and sustained gonadotropin-releasing hormone (GnRH) receptor signaling. J. Biol. Chem. *284*, 35746–35757. https://doi.org/10.1074/jbc.m109.063917.

Aycan, Z., Savaş-Erdeve, Ş., Çetinkaya, S., Kurnaz, E., Keskin, M., Muratoğlu Şahin, N., Bayramoğlu, E., and Ceylaner, G. (2018). Investigation of MKRN3 mutation in patients with familial central precocious puberty. J. Clin. Res. Pediatr. Endocrinol. *10*, 223–229. https://doi.org/10.4274/jcrpe.5506.

Blanpied, T.A., Scott, D.B., and Ehlers, M.D. (2003). Age-related regulation of dendritic endocytosis associated with altered clathrin dynamics. Neurobiol. Aging *24*, 1095–1104. https://doi.org/10.1016/j.neurobiolaging.2003.04.004.

Bramble, M.S., Goldstein, E.H., Lipson, A., Ngun, T., Eskin, A., Gosschalk, J.E., Roach, L., Vashist, N., Barseghyan, H., Lee, E., et al. (2016). A novel follicle-stimulating hormone receptor mutation causing primary ovarian failure: a fertility application of whole exome sequencing. Hum. Reprod. *31*, 905–914. https://doi.org/10.1093/humrep/dew025.

Brinkman, E.K., Chen, T., Amendola, M., and van Steensel, B. (2014). Easy quantitative assessment of genome editing by sequence trace decomposition. Nucleic Acids Res. *42*, e168. https://doi.org/10.1093/nar/gku936.

Bruysters, M., Christin-Maitre, S., Verhoef-Post, M., Sultan, C., Auger, J., Faugeron, I., Larue, L., Lumbroso, S., Themmen, A.P.N., and Bouchard, P. (2008). A new LH receptor splice mutation responsible for male hypogonadism with

subnormal sperm production in the propositus, and infertility with regular cycles in an affected sister. Hum. Reprod. 23, 1917–1923. https://doi.org/10.1093/humrep/den180.

Byers, S.L., Wiles, M.V., Dunn, S.L., and Taft, R.A. (2012). Mouse estrous cycle identification tool and images. PLoS One 7, e35538. https://doi.org/10.1371/journal.pone.0035538.

Calandra, C.R., Mocarbel, Y., Vishnopolska, S.A., Toneguzzo, V., Oliveri, J., Cazado, E.C., Biagioli, G., Turjanksi, A.G., and Marti, M. (2019). Gordon Holmes syndrome caused by RNF216 novel mutation in 2 argentinean siblings. Mov. Disord. Clin. Pract. 6, 259–262. https://doi.org/10.1002/mdc3.12721.

Carpenter, A.E., Jones, T.R., Lamprecht, M.R., Clarke, C., Kang, I.H., Friman, O., Guertin, D.A., Chang, J.H., Lindquist, R.A., Moffat, J., et al. (2006). CellProfiler: image analysis software for identifying and quantifying cell phenotypes. Genome Biol. 7, R100. https://doi.org/10.1186/gb-2006-7-10-r100.

Chuang, T.-H., and Ulevitch, R.J. (2004). Erratum: Triad3A, an E3 ubiquitin-protein ligase regulating Toll-like receptors. Nat. Immunol. 5, 968. https://doi.org/10.1038/ni0904-968.

Cotton, T.R., Cobbold, S.A., Bernardini, J.P., Richardson, L.W., Wang, X.S., and Lechtenberg, B.C. (2022). Structural basis of K63-ubiquitin chain formation by the Gordon-Holmes syndrome RBR E3 ubiquitin ligase RNF216. Mol. Cell 82, 598–615.e8. https://doi.org/10.1016/j.molcel.2021.12.005.

Cottrell, E.C., Campbell, R.E., Han, S.-K., and Herbison, A.E. (2006). Postnatal remodeling of dendritic structure and spine density in gonadotropin-releasing hormone neurons. Endocrinology 147, 3652–3661. https://doi.org/10.1210/en.2006-0296.

Coutant, R., Biette-Demeneix, E., Bouvattier, C., Bouhours-Nouet, N., Gatelais, F., Dufresne, S., Rouleau, S., and Lahlou, N. (2010). Baseline inhibin B and anti-Mullerian hormone measurements for diagnosis of hypogonadotropic hypogonadism (HH) in boys with delayed puberty. J. Clin. Endocrinol. Metab. 95, 5225–5232. https://doi.org/10.1210/jc.2010-1535.

de Roux, N., Genin, E., Carel, J.-C., Matsuda, F., Chaussain, J.-L., and Milgrom, E. (2003). Hypogonadotropic hypogonadism due to loss of function of the KiSS1-derived peptide receptor GPR54. Proc. Natl. Acad. Sci. U S A 100, 10972–10976. https://doi.org/10.1073/pnas.1834399100.

de Roux, N., Young, J., Misrahi, M., Genet, R., Chanson, P., Schaison, G., and Milgrom, E. (1997). A family with hypogonadotropic hypogonadism and mutations in the gonadotropin-releasing hormone receptor. N. Engl. J. Med. 337, 1597–1603. https://doi.org/10.1056/nejm199711273372205.

de Vries, L., Gat-Yablonski, G., Dror, N., Singer, A., and Phillip, M. (2014). A novel MKRN3 missense mutation causing familial precocious puberty. Hum. Reprod. 29, 2838–2843. https://doi.org/10.1093/humrep/deu256.

Fearns, C., Pan, Q., Mathison, J.C., and Chuang, T.-H. (2006). Triad3A regulates ubiquitination and proteasomal degradation of RIP1 following disruption of HSP90 binding. J. Biol. Chem. 281, 34592–34600. https://doi.org/10.1074/jbc.m604019200.

Ganos, C., Hersheson, J., Adams, M., Bhatia, K.P., and Houlden, H. (2015). Syndromic associations and RNF216 mutations. Park. Relat. Disord. 21, 1389–1390. https://doi.org/10.1016/j.parkreldis.2015.09.010.

George, A.J., Hoffiz, Y.C., Charles, A.J., Zhu, Y., and Mabb, A.M. (2018). A comprehensive atlas of E3 ubiquitin ligase mutations in neurological disorders. Front. Genet. 9, 29. https://doi.org/10.3389/fgene.2018.00029.

Giuliano, C.J., Lin, A., Girish, V., and Sheltzer, J.M. (2019). Generating single cell-derived knockout clones in mammalian cells with CRISPR/Cas9. Curr. Protoc. Mol. Biol. 128, e100. https://doi.org/10.1002/cpmb.100.

Grandone, A., Cirillo, G., Sasso, M., Capristo, C., Tornese, G., Marzuillo, P., Luongo, C., Rosaria Umano, G., Festa, A., Coppola, R., et al. (2018). MKRN3 levels in girls with central precocious puberty and correlation with sexual hormone levels: a pilot study. Endocrine 59, 203–208. https://doi.org/10.1007/s12020-017-1281-x.

Groome, N.P., Illingworth, P.J., O'Brien, M., Pai, R., Rodger, F.E., Mather, J.P., and McNeilly, A.S. (1996). Measurement of dimeric inhibin B throughout the human menstrual cycle. J. Clin. Endocrinol. Metab. 81, 1401–1405. https://doi.org/10.1210/jc.81.4.1401.

Han, S.-K., Gottsch, M.L., Lee, K.J., Popa, S.M., Smith, J.T., Jakawich, S.K., Clifton, D.K., Steiner, R.A., and Herbison, A.E. (2005). Activation of gonadotropin-releasing hormone neurons by kisspeptin as a neuroendocrine switch for the onset of puberty. J. Neurosci. 25, 11349–11356. https://doi.org/10.1523/jneurosci.3328-05.2005.

Hanamsagar, R., Alter, M.D., Block, C.S., Sullivan, H., Bolton, J.L., and Bilbo, S.D. (2017). Generation of a microglial developmental index in mice and in humans reveals a sex difference in maturation and immune reactivity. Glia 66, 460. https://doi.org/10.1002/glia.23277.

Hardelin, J.-P. (2001). Kallmann syndrome: towards molecular pathogenesis. Mol. Cell Endocrinol. 179, 109–121. https://doi.org/10.1159/000060865.

Harris, G.W. (1955). Neural Control of the Pituitary Gland (E. Arnold).

Hayer, S.N., Deconinck, T., Bender, B., Smets, K., Züchner, S., Reich, S., Schöls, L., Schüle, R., De Jonghe, P., Baets, J., et al. (2017). STUB1/CHIP mutations cause Gordon Holmes syndrome as part of a widespread multisystemic neurodegeneration: evidence from four novel mutations. Orphanet J. Rare Dis. 12, 31. https://doi.org/10.1186/s13023-017-0580-x.

Herbison, A.E. (2016). Control of puberty onset and fertility by gonadotropin-releasing hormone neurons. Nat. Rev. Endocrinol. 12, 452–466. https://doi.org/10.1038/nrendo.2016.70.

Hershko, A., and Ciechanover, A. (1998). The ubiquitin system. Annu. Rev. Biochem. 67, 425–479. https://doi.org/10.1146/annurev.biochem.67.1.425.

Holmes, G. (1908). A form of familial degeneration of the cerebellum. Brain 30, 466–489. https://doi.org/10.1093/brain/30.4.466.

Husain, N., Yuan, Q., Yen, Y.C., Pletnikova, O., Sally, D.Q., Worley, P., Bichler, Z., and Shawn Je, H. (2017). TRIAD3/RNF216 mutations associated with Gordon Holmes syndrome lead to synaptic and cognitive impairments via Arc misregulation. Aging Cell 16, 281–292. https://doi.org/10.1111/acel.12551.

Jasoni, C.L., Porteous, R.W., and Herbison, A.E. (2009). Anatomical location of mature GnRH neurons corresponds with their birthdate in the developing mouse. Dev. Dyn. 238, 524–531. https://doi.org/10.1002/dvdy.21869.

Kalantaridou, S.N., and Chrousos, G.P. (2002). Monogenic disorders of puberty. J. Clin. Endocrinol. Metab. 87, 2481–2494. https://doi.org/10.1210/jcem.87.6.8668.

Kile, J.P., and Nett, T.M. (1994). Differential secretion of follicle-stimulating hormone and luteinizing hormone from ovine pituitary cells following activation of protein kinase A, protein kinase C, or increased intracellular Calcium1. Biol. Reprod. 50, 49–54. https://doi.org/10.1095/biolreprod50.1.49.

Kim, Y.H., Kwak, M.S., Shin, J.M., Hayuningtyas, R.A., Choi, J.E., and Shin, J.-S. (2018). Inflachromene inhibits autophagy through modulation of Beclin 1 activity. J. Cell Sci. 131, jcs211201. https://doi.org/10.1242/jcs.211201.

Komander, D., and Rape, M. (2012). The ubiquitin code. Annu. Rev. Biochem. 81, 203–229. https://doi.org/10.1146/annurev-biochem-060310-170328.

Kotani, M., Detheux, M., Vandenbogaerde, A., Communi, D., Vanderwinden, J.-M., Le Poul, E., Brézillon, S., Tyldesley, R., Suarez-Huerta, N., Vandeput, F., et al. (2001). The metastasis suppressor gene KiSS-1 encodes kisspeptins, the natural ligands of the orphan G protein-coupled receptor GPR54. J. Biol. Chem. 276, 34631–34636. https://doi.org/10.1074/jbc.m104847200.

Kubini, K., Zachmann, M., Albers, N., Hiort, O., Bettendorf, M., Wölfle, J., Bidlingmaier, F., and Klingmüller, D. (2000). Basal inhibin B and the testosterone response to human chorionic gonadotropin correlate in prepubertal boys. J. Clin. Endocrinol. Metab. 85, 134–138. https://doi.org/10.1210/jc.85.1.134.

Lainez, N.M., and Coss, D. (2019). Leukemia inhibitory factor represses GnRH gene expression via cFOS during inflammation in male mice. Neuroendocrinology 108, 291–307. https://doi.org/10.1159/000496754.

Lee, K., Duan, W., Sneyd, J., and Herbison, A.E. (2010). Two slow calcium-activated afterhyperpolarization currents control burst firing dynamics in gonadotropin-releasing hormone neurons. J. Neurosci. 30, 6214–6224. https://doi.org/10.1523/jneurosci.6156-09.2010.

Lenz, K.M., Nugent, B.M., Haliyur, R., and McCarthy, M.M. (2013). Microglia are essential to masculinization of brain and behavior.

J. Neurosci. *33*, 2761–2772. https://doi.org/10.1523/jneurosci.1268-12.2013.

Li, D., Li, F., Meng, L., Wei, H., Zhang, Q., Jiang, F., Chen, D.N., Li, W., Tan, Y.Q., and Li, J.D. (2021). RNF216 regulates meiosis and PKA stability in the testes. FASEB J. *35*, e21460. https://doi.org/10.1096/fj.202002294rr.

Li, F., Li, D., Liu, H., Cao, B.-B., Jiang, F., Chen, D.-N., and Li, J.-D. (2019). RNF216 regulates the migration of immortalized GnRH neurons by suppressing Beclin1-mediated autophagy. Front. Endocrinol. *10*, 12. https://doi.org/10.3389/fendo.2019.00012.

Lieto, M., Galatolo, D., Roca, A., Cocozza, S., Pontillo, G., Fico, T., Pane, C., Saccà, F., De Michele, G., Santorelli, F.M., et al. (2019). Overt hypogonadism may not Be a sentinel sign of RING finger protein 216: two novel mutations associated with ataxia, chorea, and fertility. Mov. Disord. Clin. Pract. *6*, 724–726. https://doi.org/10.1002/mdc3.12839.

Liu, H., Kong, X., and Chen, F. (2017). Mkrn3 functions as a novel ubiquitin E3 ligase to inhibit Nptx1 during puberty initiation. Oncotarget *8*, 85102–85109. https://doi.org/10.18632/oncotarget.19347.

Livak, K., and Schmittgen, T. (2001). Analysis of Relative Gene Expression Data Using Real-Time Quantitative PCR and the $2^{-\Delta\Delta C_T}$ Method. Methods *25*, In this issue, 402–408. In this issue. https://doi.org/10.1006/meth.2001.1262.

Luisi, S., Florio, P., Reis, F.M., and Petraglia, F. (2005). Inhibins in female and male reproductive physiology: role in gametogenesis, conception, implantation and early pregnancy. Hum. Reprod. Update *11*, 123–135. https://doi.org/10.1093/humupd/dmh057.

Mabb, A.M., Je, H.S., Wall, M.J., Robinson, C.G., Larsen, R.S., Qiang, Y., Corrêa, S.A.L., and Ehlers, M.D. (2014). Triad3A regulates synaptic strength by ubiquitination of arc. Neuron *82*, 1299–1316. https://doi.org/10.1016/j.neuron.2014.05.016.

Mahesh, V.B., Zamorano, P., De Sevilla, L., Lewis, D., and Brann, D.W. (1999). Characterization of ionotropic glutamate receptors in rat hypothalamus, pituitary and immortalized gonadotropin-releasing hormone (GnRH) neurons (GT1-7 cells). Neuroendocrinology *69*, 397–407. https://doi.org/10.1159/000054442.

Margolin, D.H., Kousi, M., Chan, Y.M., Lim, E.T., Schmahmann, J.D., Hadjivassiliou, M., Hall, J.E., Adam, I., Dwyer, A., Plummer, L., et al. (2013). Ataxia, dementia, and hypogonadotropism caused by disordered ubiquitination. N. Engl. J. Med. *368*, 1992–2003. https://doi.org/10.1056/nejmoa1215993.

Meachem, S.J., Nieschlag, E., and Simoni, M. (2001). Inhibin B in male reproduction: pathophysiology and clinical relevance. Eur. J. Endocrinol. *145*, 561–571. https://doi.org/10.1530/eje.0.1450561.

Mehmood, S., Hoggard, N., and Hadjivassiliou, M. (2017). Gordon Holmes syndrome: finally genotype meets phenotype. Pract. Neurol. *17*, 476–478. https://doi.org/10.1136/practneurol-2017-001674.

Mellon, P.L., Windle, J.J., Goldsmith, P.C., Padula, C.A., Roberts, J.L., and Weiner, R.I. (1990). Immortalization of hypothalamic GnRH by genetically targeted tumorigenesis. Neuron *5*, 1–10. https://doi.org/10.1016/0896-6273(90)90028-e.

Melnick, A.F., Gao, Y., Liu, J., Ding, D., Predom, A., Kelly, C., Hess, R.A., and Chen, C. (2019). RNF216 is essential for spermatogenesis and male fertility†. Biol. Reprod. *100*, 1132–1134. https://doi.org/10.1093/biolre/ioz006.

Moenter, S.M., Anthony DeFazio, R., Pitts, G.R., and Nunemaker, C.S. (2003). Mechanisms underlying episodic gonadotropin-releasing hormone secretion. Front. Neuroendocrinol. *24*, 79–93. https://doi.org/10.1016/s0091-3022(03)00013-x.

Nakhaei, P., Mesplede, T., Solis, M., Sun, Q., Zhao, T., Yang, L., Chuang, T.-H., Ware, C.F., Lin, R., and Hiscott, J. (2009). The E3 ubiquitin ligase Triad3A negatively regulates the RIG-I/MAVS signaling pathway by targeting TRAF3 for degradation. PLoS Pathog. *48*, e1000650. https://doi.org/10.1016/j.cyto.2009.07.540.

Nuruddin, S., Syverstad, G.H.E., Lillehaug, S., Leergaard, T.B., Nilsson, L.N.G., Ropstad, E., Krogenæs, A., Haraldsen, I.R.H., and Torp, R. (2014). Elevated mRNA-levels of gonadotropin-releasing hormone and its receptor in plaque-bearing Alzheimer's disease transgenic mice. PLoS One *9*, e103607. https://doi.org/10.1371/journal.pone.0103607.

Otani, H., Otsuka, F., Takeda, M., Mukai, T., Terasaka, T., Miyoshi, T., Inagaki, K., Suzuki, J., Ogura, T., Lawson, M.A., et al. (2009). Regulation of GNRH production by estrogen and bone morphogenetic proteins in GT1-7 hypothalamic cells. J. Endocrinol. *203*, 87–97. https://doi.org/10.1677/joe-09-0065.

Pellegrino, G., Martin, M., Allet, C., Lhomme, T., Geller, S., Franssen, D., Mansuy, V., Manfredi-Lozano, M., Coutteau-Robles, A., Delli, V., et al. (2021). GnRH neurons recruit astrocytes in infancy to facilitate network integration and sexual maturation. Nat. Neurosci. *24*, 1660–1672. https://doi.org/10.1038/s41593-021-00960-z.

Plant, T.M. (2015). 60 years of neuroendocrinology: the hypothalamo-pituitary-gonadal axis. J. Endocrinol. *226*, T41–T54. https://doi.org/10.1530/joe-15-0113.

Plant, T.M., and Marshall, G.R. (2001). The functional significance of FSH in spermatogenesis and the control of its secretion in male primates. Endocr. Rev. *22*, 764–786. https://doi.org/10.1210/edrv.22.6.0446.

Quinton, R., Barnett, P., Coskeran, P., and Bouloux, P.-M.G. (1999). Gordon Holmes spinocerebellar ataxia: a gonadotrophin deficiency syndrome resistant to treatment with pulsatile gonadotrophin-releasing hormone. Clin. Endocrinol. *51*, 525–529. https://doi.org/10.1046/j.1365-2265.1999.00859.x.

Ransohoff, R.M., and Perry, V.H. (2009). Microglial physiology: unique stimuli, specialized responses. Annu. Rev. Immunol. *27*, 119–145. https://doi.org/10.1146/annurev.immunol.021908.132528.

Reddish, F.N., Miller, C.L., Deng, X., Dong, B., Patel, A.A., Ghane, M.A., Mosca, B., McBean, C., Wu, S., Solntsev, K.M., et al. (2021). Rapid subcellular calcium responses and dynamics by calcium sensor G-CatchER+. iScience *24*, 102129. https://doi.org/10.1016/j.isci.2021.102129.

Rønnekleiv, O.K., and Kelly, M.J. (2013). Kisspeptin excitation of GnRH neurons. Adv. Exp. Med. Biol. *784*, 113–131. https://doi.org/10.1007/978-1-4614-6199-9_6.

Roper, L.K., Briguglio, J.S., Evans, C.S., Jackson, M.B., and Chapman, E.R. (2015). Sex-specific regulation of follicle-stimulating hormone secretion by synaptotagmin 9. Nat. Commun. *6*, 8645. https://doi.org/10.1038/ncomms9645.

Santens, P., Van Damme, T., Steyaert, W., Willaert, A., Sablonnière, B., De Paepe, A., Coucke, P.J., and Dermaut, B. (2015). RNF216 mutations as a novel cause of autosomal recessive Huntington-like disorder. Neurology *84*, 1760–1766. https://doi.org/10.1212/wnl.0000000000001521.

Santi, D., Crépieux, P., Reiter, E., Spaggiari, G., Brigante, G., Casarini, L., Rochira, V., and Simoni, M. (2020). Follicle-stimulating hormone (FSH) action on spermatogenesis: a focus on physiological and therapeutic roles. J. Clin. Med. *9*, 1014. https://doi.org/10.3390/jcm9041014.

Sawyer, S.L., Schwartzentruber, J., Beaulieu, C.L., Dyment, D., Smith, A., Warman Chardon, J., Yoon, G., Rouleau, G.A., Suchowersky, O., Siu, V., et al. (2014). Exome sequencing as a diagnostic tool for pediatric-onset ataxia. Hum. Mutat. *35*, 45–49. https://doi.org/10.1002/humu.22451.

Schwarz, J.M., Sholar, P.W., and Bilbo, S.D. (2012). Sex differences in microglial colonization of the developing rat brain. J. Neurochem. *120*, 948–963. https://doi.org/10.1111/j.1471-4159.2011.07630.x.

Schwenk, F., Baron, U., and Rajewsky, K. (1995). A cre-transgenic mouse strain for the ubiquitous deletion of loxP-flanked gene segments including deletion in germ cells. Nucleic Acids Res. *23*, 5080–5081. https://doi.org/10.1093/nar/23.24.5080.

Schwintzer, L., Aguado Roca, E., and Broemer, M. (2019). TRIAD3/RNF216 E3 ligase specifically synthesises K63-linked ubiquitin chains and is inactivated by mutations associated with Gordon Holmes syndrome. Cell Death Discov. *5*, 75. https://doi.org/10.1038/s41420-019-0158-6.

Seenivasan, R., Hermanns, T., Blyszcz, T., Lammers, M., Praefcke, G.J.K., and Hofmann, K. (2019). Mechanism and chain specificity of RNF216/TRIAD3, the ubiquitin ligase mutated in Gordon Holmes syndrome. Hum. Mol. Genet. *28*, 2862–2873. https://doi.org/10.1093/hmg/ddz098.

Seminara, S.B., Acierno, J.S., Abdulwahid, N.A., Crowley, W.F., and Margolin, D.H. (2002). Hypogonadotropic hypogonadism and cerebellar ataxia: detailed phenotypic characterization of a large, extended kindred. J. Clin. Endocrinol. Metab. *87*, 1607–1612. https://doi.org/10.1210/jcem.87.4.8384.

Seminara, S.B., Messager, S., Chatzidaki, E.E., Thresher, R.R., Acierno, J.S., Shagoury, J.K., Bo-Abbas, Y., Kuohung, W., Schwinof, K.M.,

Hendrick, A.G., et al. (2003). The GPR54 gene as a regulator of puberty. N. Engl. J. Med. 349, 1614–1627. https://doi.org/10.1056/nejmoa035322.

Shalem, O., Sanjana, N.E., Hartenian, E., Shi, X., Scott, D.A., Mikkelson, T., Heckl, D., Ebert, B.L., Root, D.E., Doench, J.G., et al. (2014). Genome-scale CRISPR-Cas9 knockout screening in human cells. Science 343, 84–87. https://doi.org/10.1126/science.1247005.

Sharif, A., Baroncini, M., and Prevot, V. (2013). Role of Glia in the regulation of gonadotropin-releasing hormone neuronal activity and secretion. Neuroendocrinology 98, 1–15. https://doi.org/10.1159/000351867.

Skrapits, K., Kanti, V., Savanyú, Z., Maurnyi, C., Szenci, O., Horváth, A., Borsay, B.Á., Herczeg, L., Liposits, Z., and Hrabovszky, E. (2015). Lateral hypothalamic orexin and melanin-concentrating hormone neurons provide direct input to gonadotropin-releasing hormone neurons in the human. Front. Cell Neurosci. 9, 348. https://doi.org/10.3389/fncel.2015.00348.

Song, B., Schisler, J.C., Shi, C.-H., Mao, C.-Y., Wang, Q.-Z., Wang, R.-H., Sun, S.-L., Xu, L., Tan, S., Portbury, A.L., et al. (2013). Ataxia and hypogonadism caused by the loss of ubiquitin ligase activity of the U box protein CHIP. Hum. Mol. Genet. 23, 1013–1024. https://doi.org/10.1093/hmg/ddt497.

Stecchini, M.F., Macedo, D.B., Reis, A.C.S., Abreu, A.P., Moreira, A.C., Castro, M., Kaiser, U.B., Latronico, A.C., and Antonini, S.R. (2016). Time course of central precocious puberty development caused by an MKRN3 gene mutation: a prismatic case. Horm. Res. Paediatr. 86, 126–130. https://doi.org/10.1159/000447515.

Tata, B.K., Harbulot, C., Csaba, Z., Peineau, S., Jacquier, S., and de Roux, N. (2017). Rabconnectin-3α is required for the morphological maturation of GnRH neurons and kisspeptin responsiveness. Sci. Rep. 7, 42463. https://doi.org/10.1038/srep42463.

Tilbrook, A.J., and Clarke, I.J. (2001). Negative feedback regulation of the secretion and actions of gonadotropin-releasing hormone in males. Biol. Reprod. 64, 735–742. https://doi.org/10.1095/biolreprod64.3.735.

Timmons, M., Tsokos, M., Asab, M.A., Seminara, S.B., Zirzow, G.C., Kaneski, C.R., Heiss, J.D., van der Knaap, M.S., Vanier, M.T., Schiffmann, R., et al. (2006). Peripheral and central hypomyelination with hypogonadotropic hypogonadism and hypodontia. Neurology 67, 2066–2069. https://doi.org/10.1212/01.wnl.0000247666.28904.35.

Tonsfeldt, K.J., Goodall, C.P., Latham, K.L., and Chappell, P.E. (2011). Oestrogen induces rhythmic expression of the Kisspeptin-1 receptor GPR54 in hypothalamic gonadotrophin-releasing hormone-secreting GT1-7 cells. J. Neuroendocrinol. 23, 823–830. https://doi.org/10.1111/j.1365-2826.2011.02188.x.

Tronche, F., Kellendonk, C., Kretz, O., Gass, P., Anlag, K., Orban, P.C., Bock, R., Klein, R., and Schütz, G. (1999). Disruption of the glucocorticoid receptor gene in the nervous system results in reduced anxiety. Nat. Genet. 23, 99–103. https://doi.org/10.1038/12703.

Vegeto, E., Bonincontro, C., Pollio, G., Sala, A., Viappiani, S., Nardi, F., Brusadelli, A., Viviani, B., Ciana, P., and Maggi, A. (2001). Estrogen prevents the lipopolysaccharide-induced inflammatory response in microglia. J. Neurosci. 21, 1809–1818. https://doi.org/10.1523/jneurosci.21-06-01809.2001.

Wall, M.J., Collins, D.R., Chery, S.L., Allen, Z.D., Pastuzyn, E.D., George, A.J., Nikolova, V.D., Moy, S.S., Philpot, B.D., Shepherd, J.D., et al. (2018). The temporal dynamics of arc expression regulate cognitive flexibility. Neuron 98, 1124–1132.e7. https://doi.org/10.1016/j.neuron.2018.05.012.

Wang, H., Wang, Y., Qian, L., Wang, X., Gu, H., Dong, X., Huang, S., Jin, M., Ge, H., Xu, C., et al. (2016). RNF216 contributes to proliferation and migration of colorectal cancer via suppressing BECN1-dependent autophagy. Oncotarget 7, 51174–51183. https://doi.org/10.18632/oncotarget.9433.

Watanabe, M., Sakuma, Y., and Kato, M. (2004). High expression of the R-type voltage-gated Ca2+ channel and its involvement in Ca2+-dependent gonadotropin-releasing hormone release in GT1–7 cells. Endocrinology 145, 2375–2383. https://doi.org/10.1210/en.2003-1257.

Welt, C.K., Martin, K.A., Taylor, A.E., Lambert-Messerlian, G.M., Crowley, W.F., Jr., Smith, J.A., Schoenfeld, D.A., and Hall, J.E. (1997). Frequency modulation of follicle-stimulating hormone (FSH) during the luteal-follicular transition: evidence for FSH control of inhibin B in normal women. J. Clin. Endocrinol. Metab. 82, 2645–2652. https://doi.org/10.1210/jc.82.8.2645.

Wetsel, W.C., Eraly, S.A., Whyte, D.B., and Mellon, P.L. (1993). Regulation of gonadotropin-releasing hormone by protein kinase-A and -C in immortalized hypothalamic neurons. Endocrinology 132, 2360–2370. https://doi.org/10.1210/endo.132.6.8504741.

Wetsel, W.C., and Negro-Vilar, A. (1989). Testosterone selectively influences protein kinase-C-coupled secretion of proluteinizing hormone-releasing hormone-derived peptides.

Endocrinology 125, 538–547. https://doi.org/10.1210/endo-125-1-538.

Weyler, R.T., Yurko-Mauro, K.A., Rubenstein, R., Kollen, W.J.W., Reenstra, W., Altschuler, S.M., Egan, M., and Mulberg, A.E. (1999). CFTR is functionally active in GnRH-expressing GT1–7 hypothalamic neurons. Am. J. Physiol. 277, C563–C571. https://doi.org/10.1152/ajpcell.1999.277.3.c563.

Wu, J., Liu, L., Matsuda, T., Zhao, Y., Rebane, A., Drobizhev, M., Chang, Y.F., Araki, S., Arai, Y., March, K., et al. (2013). Improved orange and red $Ca^2\pm$ indicators and photophysical considerations for optogenetic applications. ACS Chem. Neurosci. 4, 963–972. https://doi.org/10.1021/cn400012b.

Xu, C., Feng, K., Zhao, X., Huang, S., Cheng, Y., Qian, L., Wang, Y., Sun, H., Jin, M., Chuang, T.-H., et al. (2014). Regulation of autophagy by E3 ubiquitin ligase RNF216 through BECN1 ubiquitination. Autophagy 10, 2239–2250. https://doi.org/10.4161/15548627.2014.981792.

Yoshida, S., Plant, S., Taylor, P.L., and Eidne, K.A. (1989). Chloride channels mediate the response to gonadotropin-releasing hormone (GnRH) in Xenopus oocytes injected with rat anterior pituitary mRNA. Mol. Endocrinol. 3, 1953–1960. https://doi.org/10.1210/mend-3-12-1953.

Zhang, C., Bosch, M.A., Rick, E.A., Kelly, M.J., and Rønnekleiv, O.K. (2009). 17 -Estradiol regulation of T-type calcium channels in gonadotropin-releasing hormone neurons. J. Neurosci. 29, 10552–10562. https://doi.org/10.1523/jneurosci.2962-09.2009.

Zhang, C., Roepke, T.A., Kelly, M.J., and Rønnekleiv, O.K. (2008). Kisspeptin depolarizes gonadotropin-releasing hormone neurons through activation of TRPC-like cationic channels. J. Neurosci. 28, 4423–4434. https://doi.org/10.1523/jneurosci.5352-07.2008.

Zhang, G., Li, J., Purkayastha, S., Tang, Y., Zhang, H., Yin, Y., Li, B., Liu, G., and Cai, D. (2013). Hypothalamic programming of systemic ageing involving IKK-β, NF-κB and GnRH. Nature 497, 211–216. https://doi.org/10.1038/nature12143.

Zheng, N., and Shabek, N. (2017). Ubiquitin ligases: structure, function, and regulation. Annu. Rev. Biochem. 86, 129–157. https://doi.org/10.1146/annurev-biochem-060815-014922.

Zimmerman, L., Parr, B., Lendahl, U., Cunningham, M., McKay, R., Gavin, B., Mann, J., Vassileva, G., and McMahon, A. (1994). Independent regulatory elements in the nestin gene direct transgene expression to neural stem cells or muscle precursors. Neuron 12, 11–24. https://doi.org/10.1016/0896-6273(94)90148-1.

STAR★METHODS

KEY RESOURCES TABLE

REAGENT or RESOURCE	SOURCE	IDENTIFIER
Antibodies		
Rat polyclonal anti-GnRH	Erik Hrabovszky, Laboratory of Reproductive Neurobiology, Institute of Experimental Medicine, Budapest Hungary	N/A
Guinea Pig polyclonal anti-NeuN	EMD Millipore	Cat#ABN90P, RRID: AB_2341095
Donkey anti-rat Alexa Fluor 488	Jackson ImmunoResearch Laboratories	Cat#712-545-153, RRID: AB_2340684
Donkey anti-guinea pig Alexa Fluor 647	VWR	Cat#706-605-148, RRID: AB_2340476
DAPI (4′,6-Diamidino-2-Phenylindole, Dihydrochloride)	ThermoFisher Scientific	Cat #62248, RRID: AB_2629482
Goat anti-Iba1	Novus Biologicals	Cat#NB100-1028; RRID: AB_521594
Goat anti-GFAP	Abcam	Cat#ab53554, RRID: AB_880202
Donkey anti-Goat biotin-SP	Jackson ImmunoResearch	Cat#705-065-147, RRID: AB_2340397
Rabbit polyclonal anti-RNF216	Bethyl Laboratories	Cat #A304-111A, RRID: AB_2621360
Rabbit anti-KISS1/GPR54	Lifespan Biosciences	Cat#LS-B15332
Rabbit anti-GNRHR	Lifespan Biosciences	Cat# LS-C383737
Rabbit anti-Arc	Synaptic Systems	Cat#156 003, RRID: AB_887694
Rabbit anti-GFP	Novus Biologicals	Cat#NB600-308, RRID: AB_10003058
Mouse anti-β-Actin	Genetex	Cat #GTX629630, RRID: AB_2728646
IRDye 680RD Goat anti-Mouse IgG (H+L)	Li-COR Biosciences	Cat #926-68070, RRID: AB_10956588
IRDye 800CW Goat anti-Rabbit IgG (H+L)	Li-COR Biosciences	Cat#926-32211, RRID: AB_621843
Biological samples		
Blood sera	This paper, ELISA	N/A
Brain tissue	This paper, Western blot and imaging	N/A
Female vaginal cells	This paper, cytology	N/A
Chemicals, peptides, and recombinant proteins		
DMEM (Dulbeccos Modification of Eagle Medium)	Corning, Inc.	Cat#10-013-CV
Fetal Bovine Serum	Corning, Inc.	Cat#35-016-CV
Penicillin-Streptomycin	ThermoFischer Scientific, Inc.	Cat#15070063
Trypsin-EDTA (0.25%), Phenol red	ThermoFischer Scientific, Inc.	Cat#25200056
DPBS (Dulbecco's Phosphate-Buffered Saline)	ThermoFischer Scientific, Inc.	Cat#14-190-250
Halt™ Phosphatase Inhibitor Cocktail	ThermoFischer Scientific, Inc.	Cat#Pl78420
Odyssey Blocking Buffer	Li-COR Biosciences, Inc.	Cat#927-50003
Goat Serum, New Zealand origin, Standard	ThermoFischer Scientific, Inc.	Cat#16-210-072
Poly-D-lysine hydrobromide	Sigma-Aldrich, Inc.	Cat#P7280
Paraformaldehyde	Electron Microscopy Sciences	Cat#19210
M-1 Embedding Matrix	ThermoFischer Scientific, Inc.	Cat#1310
Fluoro-Gel, (with Tris Buffer)	Electron Microscopy Sciences	Cat#102092-122
Permount mounting media	ThermoFischer Scientific, Inc.	SP15-500
Puromycin dihydrochloride	Sigma-Aldrich, Inc.	Cat#P8833
3,3′-diaminobenzidine (DAB)	Sigma-Aldrich, Inc.	Cat#D5637

Continued

REAGENT or RESOURCE	SOURCE	IDENTIFIER
Critical commercial assays		
RNeasy Lipid Tissue Mini Kit	QIAGEN, Inc.	Cat#74804
Plasmid Maxi Kit	QIAGEN, Inc.	Cat#12163
Vectastain Elite ABC-HRP Kit	Vector Laboratories	Cat#PK6100
QIAquick Gel Extraction Kit	QIAGEN, Inc.	Cat#28704
Lipofectamine 2000 Transfection Reagent	ThermoFischer Scientific, Inc.	Cat#11668030
Lipofectamine 3000 Transfection Reagent	ThermoFischer Scientific, Inc.	Cat#L3000008
DNeasy Blood & Tissue Kit	QIAGEN, Inc.	Cat#69504
QIAquick PCR & Gel Cleanup Kit	QIAGEN, Inc.	Cat#28506
iScript Reverse Transcription Supermix for RT-qPCR	Bio-Rad, Inc.	Cat#1708840
FastStart Essential DNA Green Master Mix	Roche Diagnostics	Cat#6402712001
GnRH ELISA	Cusabio, Inc.	Cat#CSB-E08152m
Revert 700 total protein stain	Li-COR Biosciences, Inc.	Cat#926-11016
Pierce 660nM Protein Assay Kit	ThermoFischer Scientific, Inc.	Cat#22662
Quick Ligation Kit	New England BioLabs	Cat#101227-656
Experimental models: Cell lines		
GT1-7 cells	Pamella Mellon, The Salk Institute for Biological Sciences	N/A
Experimental models: Organisms/strains		
Mouse: *CMV::Rnf216/Triad3*^{−/−}: C57BL/6N-Rnf216<tm1c(EUCOMM) Wtsi *Rnf216/Triad3*^{fl/fl}	Canadian Mouse Mutant Repository at the Hospital for Sick Children, Toronto, CA	MGI: 6316263
Mouse: *CMV::Rnf216/Triad3*^{−/−}: B6. C-Tg(CMV-cre)1Cgn/J. *CMV*-CRE^{+/+}	The Jackson Laboratory	JAX stock #006054
Mouse: *Nestin::Rnf216/Triad3*^{−/−}: B6. Cg-Tg(Nes-cre)1Kln/J. *Nestin*-CRE^{−/+}	The Jackson Laboratory	JAX stock # 003771
Oligonucleotides		
CRISPR A-F 5′-CACCGTCAGT AGATGACCAGCTAAT-3′	This paper, cloning	N/A
CRISPR A-F 5′-CACCGTCAGT AGATGACCAGCTAAT-3′	This paper, cloning	N/A
CRISPR B-F 5′-CACCGGAACAA CTTTCCCTGCCACC-3′	This paper, cloning	N/A
CRISPR B-R 5′-AAACGGTGGCAG GGAAAGTTGTTCC-3′	This paper, cloning	N/A
CRISPR A-F 5′-ATGGCGGAAAA ACATTGGGC-3′	This paper, sequencing	N/A
CRISPR A-R 5′-ACCTGGACCAA GCAGTAAGC-3′	This paper, sequencing	N/A
CRISPR B-F 5′-AACAGTAGAATCG CTCTGGCT-3′	This paper, sequencing	N/A
CRISPR B-R 5′-CTTGTTTTTCA AACCCTGCAGAAC-3′	This paper, sequencing	N/A
PrimePCR™ SYBR® Green Assay: Tnf, Mouse	Bio-Rad, Inc.	Cat#10025636
PrimePCR™ SYBR® Green Assay: Il1b, Mouse	Bio-Rad, Inc.	Cat#10025636

Continued

REAGENT or RESOURCE	SOURCE	IDENTIFIER
Recombinant DNA		
LentiCRISPR-*Rnf216/Triad3* CrisprA	This paper, cloning	N/A
LentiCRISPR-*Rnf216/Triad3* CrisprB	This paper, cloning	N/A
pcDNA3.1(+)-N-eGFP-RNF216/TRIAD3 Isoform A	This paper, cloning	N/A
pcDNA3.1(+)-N-eGFP-RNF216/TRIAD3 Isoform B	This paper, cloning	N/A
pRK5FLAG-Triad3A-WT	Dr. Tsung-Hsien Chuang, Chuang and Ulevitch, 2004	N/A
pRK5FLAG-Triad3A-CA	This paper, cloning	N/A
pLentilox3.7-Scramble-shRNA	Mabb et al., 2014	N/A
pLentilox3.7-*Triad3*-shRNA	Mabb et al., 2014	N/A
CMV-R-GECO1.2	Wu et al., 2013	Addgene #45494
LentiCRISPR	Shalem et al., 2014	Cat#pXPR_001
Software and algorithms		
ImageJ	NIH	https://imagej.nih.gov/ij/; RRID: SCR_003070
FIJI (Fiji is Just ImageJ)	NIH	http://fiji.sc/; RRID: SCR_002285
Matlab	The MathWorks, Inc.	RRID: SCR_001622
Prism	GraphPad	RRID: SCR_002798
Tracking of Indels by DEcomposition (TIDE)	Brinkman et al., 2014	https://tide.nki.nl/
Cell Profiler	Broad Institute	https://cellprofiler.org/; RRID: SCR_007358

RESOURCE AVAILABILITY

Lead contact

Further information and requests for resources and reagents should be directed to and will be fulfilled by the lead contact, Angela Mabb (amabb@gsu.edu).

Materials availability

The availability of GT1-7 CRISPR lines requires initiation of a material transfer agreement (MTA) with the Salk Institute for Biological Sciences.

Plasmids generated in this study will be shared by the lead contact upon request.

Mouse lines generated in this study are all commercially available.

Data and code availability

All data reported in this paper will be shared by the lead contact upon request.

This paper does not report original code.

Any additional information required to reanalyze data reported in this paper is available from the lead contact upon request.

EXPERIMENTAL MODEL AND SUBJECT DETAILS

Animals

Mice were kept in standard housing with littermates, provided with food and water *ad libitum*, and maintained on a 12:12 (light-dark) cycle. All behavioral tests were conducted in accordance with the National Institutes of Health Guidelines for the Use of Animals. Mice were treated in accordance with the Animal Welfare and Ethics Committee (AWERB) and experiments were performed under the appropriated project

licenses with local and national ethical approval. Samples sizes for behavior and immunohistochemistry experiments were calculated using variance from previous experiments to indicate power, which statistical analysis for significance was set at 95%. All behavioral studies and isolation of body tissue for biochemical experiments, vaginal cytology, and blood collection were approved by the Georgia State University Institutional Animal Care and Use Committee.

Generation of Rnf216/Triad3 knockout mice

Embryonic stem cell clones were generated to target exons 3 to 4 of the *Rnf216/Triad3* gene on mouse chromosome 5, which prevents the production of all isoforms (International Knockout Mouse Consortium). ES cell clones were injected into blastocytes and implanted into pseudopregnant mice. These mice were crossed to heterozygous mice for Flp recombinase to excise out the LacZ/neomycin cassette to obtain one *Rnf216* allele flanked by loxP (fl) sites to generate C57BL/6N-Rnf216<tm1c(EUCOMM)Wtsi>/Tcp (*Rnf216/Triad3*$^{wt/fl}$) (Canadian Mouse Mutant Repository at the Hospital for Sick Children, Toronto, CA). Homozygous floxed conditional male mice (*Rnf216/Triad3*$^{fl/fl}$) were crossed with homozygous *CMV-CRE*$^{+/+}$ female mice (The Jackson Laboratory, JAX stock #006054) to allow the CRE to excise out exons 3 to 4, creating a dysfunctional gene. To breed out the CRE, female offspring that were heterozygous for loxP and CRE (*Rnf216/Triad3*$^{wt/fl}$::*CMV-CRE*$^{-/+}$) were bred with WT males to generate heterozygous *Rnf216/Triad3*$^{-/+}$ mice. Male *Rnf216/Triad3*$^{-/+}$ mice were then bred with WT females to generate *Rnf216/Triad3*$^{-/+}$ mice. *Rnf216/Triad3*$^{-/+}$ male and female mice were then bred together to generate the experimental animals used for this study (*Rnf216/Triad3*$^{+/+}$ (WT), *Rnf216/Triad3*$^{-/+}$ (HET), and *Rnf216/Triad3*$^{-/-}$ (KO)). Same-sex animals were group housed unless otherwise noted. For experimental design, littermates of the same sex were randomly assigned to experimental groups. Mice were 6–8 weeks old for breeding viability experiments and 16 weeks for all other experiments.

Generation of Nestin-CRE::Rnf216/Triad3 Mice

Homozygous floxed conditional male mice (*Rnf216/Triad3*$^{fl/fl}$) were crossed with hemizygous *Nestin*-CRE$^{-/+}$ mice (The Jackson Laboratory, JAX stock # 003771) to allow the CRE to excise out exons 3 to 4, creating a dysfunctional gene selectively within neural stem/precursor cells. Offspring from this pairing, *Nestin*-CRE$^{-/+}$::*Rnf216/Triad3*$^{+/fl}$ and *Rnf216/Triad3*$^{+/fl}$ were bred together to generate male and female experimental animals for this study (*Nestin*-CRE$^{-/+}$::*Rnf216/Triad3*$^{+/+}$ (WT) and *Nestin*-CRE$^{-/+}$::*Rnf216/Triad3*$^{fl/fl}$(KO)) with the expected 1 out of 8 Mendelian ratios. Same-sex animals were group housed unless otherwise noted. For experimental design, littermates of the same sex were randomly assigned to experimental groups. Mice were 6–8 weeks old for breeding viability experiments and 16 weeks for all other experiments.

Cloning of control and Rnf216/Triad3 CRISPRs

The type II CRISPR nuclease system was implemented in GT1-7 cells to facilitate genome editing by co-expressing a codon-optimized cas9 nuclease along with a single guide RNA (sgRNA). The LentiCRISPR (pXPR_001) plasmid contains two expression cassettes, hSpCas9, and the chimeric guide RNA (Shalem et al., 2014). Briefly, 5μg of lentiviral CRISPR plasmid was digested with *BsmBI* (NEB) for 90 min at 37°C. After electrophoresis of the digested vector, the 11 kB band was gel purified using the QIAquick Gel Extraction Kit (QIAGEN) according to the manufacturer's protocol. Two sgRNA sequences targeting mouse *Rnf216/Triad3* were designed using http://crispr.mit.edu: CRISPR A (TCAGTAGATGACCAGCTAAT) which targets exon 4 and CRISPR B (GAACAACTTTCCCTGCCACC) which targets exon 2. Primer sequences are as follows:

CRISPR A-F 5′-CACCGTCAGTAGATGACCAGCTAAT-3′;

CRISPR A-R 5′-AAACATTAGCTGGTCATCTACTGAC-3′;

CRISPR B-F 5′-CACCGGAACAACTTTCCCTGCCACC-3′;

CRISPR B-R 5′-AAACGGTGGCAGGGAAAGTTGTTCC-3′.

DNA oligos were phosphorylated and annealed by mixing each oligo pair (100μM) with 10X T4 Ligation Buffer (NEB), ddH$_2$O, and T4 PNK (NEB). The reaction underwent the following cycling conditions: 37°C for 30 min, 95°C for 5 min, and then ramped down to 25°C at 0.1°C/sec. Products were then diluted 1:200 in elution buffer and finally cloned into the vector using a ligation reaction that included the *BsmBI*

digested plasmid, diluted oligo, 2X Quick Ligase Buffer (NEB), ddH$_2$O, and Quick Ligase (NEB) and incubated at room temperature for 10 min. The targeting guide sequences were transformed into *E.coli* competent cells and positive clones were sequenced for insert validation. Knockout efficiency for each targeting sequence was validated by transient transfection and immunoblotting in a B16 mouse melanoma cell line. CRISPR clones A and B were used to generate *Rnf216/Triad3* knockout clones in GT1-7 cells.

Cell culture and generation of control and Rnf216/Triad3 CRISPR clones

GT1-7 cells were a kind gift from Dr. Pamela Mellon (Mellon et al., 1990). Cells were maintained in DMEM (Corning) with 10% FBS (GE Healthcare) and 1% Pen Strep (ThermoFisher) at 37°C with 5% CO$_2$. Cells were seeded at a density of 2.5 × 10^5 cells/well in a 6-well dish and transfected with CRISPR-Cas9 plasmids using the standard Lipofectamine 3000 (Thermo Fisher) protocol. Briefly, 2.5µg of plasmid DNA was mixed with Lipofectamine 3000 reagents and incubated for 24 h before replacing with fresh media. After 48 h, 2.0 µg/mL of puromycin was added to the media for selection. After integration was established, single-cell clones were selected and expanded into colonies under puromycin selection. Loss of *Rnf216/Triad3* was validated through immunoblotting. CRISPR clones that showed a loss of RNF216/TRIAD3 were used for subsequent experiments.

Validation of CRISPR sequences

Confirmation of targeted CRISPR sequences were adapted from the Giuliano et al. protocol (Giuliano et al., 2019). GT1-7 CRISPR cells were plated at a density of 1.0 × 10^6 in a 6-well dish. Genomic DNA was extracted using the DNeasy Blood & Tissue Kit (QIAGEN) according to the manufacturer's protocol. The concentration and purity of purified DNA was assessed using a NanoDrop ND-2000/2000c (ThermoFisher). DNA was only used if it had an A260/A280 ratio between 1.8–2.0. PCR of CRISPR control, A, and B was performed using specific primer sets for CRISPR A and B. PCR products were run on a 2% agarose gel, and gel bands were manually extracted and purified using QIAquick PCR & Gel Cleanup Kit (QIAGEN) according to manufacturer's protocol. Purified PCR products were submitted to GENEWIZ (South Plainfield, NJ) for Sanger sequencing. Sequencing results were analyzed using the previously established Tracking of Indels by DEcomposition (TIDE) software (https://tide.nki.nl/) (Brinkman et al., 2014). Control CRISPR sequences were used as reference chromatograms for CRISPR A and B comparisons. Primer sequences for gRNA targeted *Rnf216/Triad3* genomic regions are as follows:

CRISPR A-F 5′-ATGGCGGAAAAACATTGGGC-3′;

CRISPR A-R 5′-ACCTGGACCAAGCAGTAAGC-3′;

CRISPR B-F 5′-AACAGTAGAATCGCTCTGGCT-3′;

CRISPR B-R 5′-CTTGTTTTTCAAACCCTGCAGAAC-3′.

METHOD DETAILS

Blood collection and ELISA

Male bedding was added to group-housed female cages 48 h before blood collection to synchronize estrous cycles and vaginal cytology was performed prior to blood collection. All mice were at 16 weeks old. Blood samples were collected (BD Microtainer Gold, ThermoFisher) at 11:00 during each session through retro-orbital bleeds, tail vein, or after decapitation and stored at room temperature for 30–60 min. Samples were then centrifuged at room temperature at 3,500 rpm for 10 min. Serum was collected and stored at −80°C until further study. Serum samples were shipped to the University of Virginia Center for Research in Reproduction, Ligand Assay and Analysis Core (supported by the Eunice Kennedy Shriver NICHDGrant R24 HD102061) for LH, FSH, and inhibin B analysis.

Vaginal cytology

Female mice at age 16 weeks that were group-housed underwent vaginal lavage with sterile Dulbecco's phosphate-buffered saline (DPBS) at 11:00 for 20 consecutive days. Cells were collected, mounted on cover slides, and stained with thionin (0.01 g/mL thionin acetate, 0.2% acetic acid, 0.007 g/mL sodium acetate anhydrous, pH 4.25) for 10 min, washed briefly with ddH$_2$O, and examined under light microscopy to determine the phase of the cycle using the classification protocol described in (Byers et al., 2012).

Breeding viability

The following pairings were set up to assess breeding viability: WT male with KO female; KO male with WT female; KO male with KO female; and HET male with HET female. Animals were between 6-8 weeks old before pairing. Females were primed with male bedding 48 hrs prior to pairing. Breeding cages contained 1 male and 1 female for a duration of 90 days. The number of litters per cage, the number of pups per litter per cage, and the number of days before the first litter were measured. The litters and pups were counted between P0-P1. These assessments also included litters and pups that did not survive through weaning at P21.

Immunohistochemistry

Male and female mice at 16 weeks old were perfused with room temperature 4% paraformaldehyde/1X PBS. Brains were collected, after being fixed in 4% PFA/1XPBS overnight at 4°C, and then placed in sucrose sinking solution (30% sucrose in 1X PBS) for 24hrs. Brains were embedded with an embedding matrix (M-1 Embedding Matrix, Thermo Fisher) and then frozen at −80°C. Embedded brains were equilibrated at −20°C for at least 1 h and then sectioned at 30 μm thickness using a cryostat (Leica CM 3050S) and stored in a freezing solution (45% PBS, 30% ethylene glycol, 25% glycerol) at −20°C. Stereological matched sections of the preoptic area, medial preoptic area, anteroventral periventricular nucleus, and arcuate nucleus were selected and washed 3x at room temperature in 1XPBS and blocked with blocking buffer (10% normal goat serum and 0.5% Triton X-100) overnight at 4°C. The following primary antibodies were added in blocking buffer and incubated for 24 h at 4°C: 1:500 dilution of Rat polyclonal anti-GnRH antibody (Skrapits et al., 2015) and 1:250 dilution Guinea Pig polyclonal anti-NeuN (EMD Millipore). After the brain slices were washed 3x with 1XPBS they were incubated with the following secondary antibodies in blocking buffer for 2 h at room temperature: 1:500 dilution of Donkey anti-rat Alexa Fluor 488 (Jackson ImmunoResearch Laboratories), 1:200 dilution of Donkey anti-guinea pig Alexa Fluor 647 (Jackson ImmunoResearch Laboratories), and 1:500 dilution of DAPI (4′,6-Diamidino-2-Phenylindole, Dihydrochloride) (ThermoFisher). The brain slices were washed 3x with 1XPBS and then mounted with mounting media (Fluoro-Gel, VWR) on coverslips (Superfrost™ Plus Microscope Slides, ThermoFisher) for imaging. Fixed slides were imaged on a laser scanning confocal microscope (Zeiss, LSM 700) using a 20x Plan-Apochromat N.A. 0.8 air objective and 40x Plan-Apochromat N.A. 1.4 oil immersion objective. GnRH signals were visualized upon excitation with a 488 nm laser, NeuN signals were visualized upon excitation with a 639 nm laser, and DAPI was visualized upon excitation with a 405 nm laser. Z-stack projections were obtained at 1μm intervals (11 slices) and images were displayed as maximum intensity projections of the entire z-series using Zeiss Zen software (Zeiss). After image collection, GnRH neurons were analyzed as described previously in (Cottrell et al., 2006) for cell soma area and the total number of dendrites projecting from the soma. GnRH neuronal morphologies were classified as described previously in (Tata et al., 2017) as mature or immature using the following criteria: unipolar/mature (one dendrite directly off the GnRH soma), bipolar/mature (two dendrites directly off the GnRH soma), or complex/immature (three or more dendritic processes directly off of the GnRH soma). Values of quantified GnRH dendritic morphologies were expressed as the percentage of the total GnRH neuron population analyzed manually using ImageJ/FIJI (NIH) software.

Iba1 and Gfap staining and imaging

Free-floating sections of male and female mice at 16 weeks old were rinsed with 3% hydrogen peroxide 2 times for 7 min each to remove any endogenous peroxidases, then washed 6 times in 1X KPBS (in mM) (1.6 NaCl, 0.4 K_2HPO_4, and 0.09 KH_2PO_4 dissolved in ddH_2O to make a 10X solution and diluted to 1X) at room temperature. Sections were then incubated overnight at room temperature in 1X KPBS containing 1.0% Triton and 1:50K dilution of Goat anti-Iba1 (Novus Biologicals) or 1:100K dilution of Goat anti-GFAP (Abcam). Sections were then washed 10 times with 1X KPBS before incubation in 1X KPBS containing 0.4% Triton and 1:600 dilution of Donkey anti-Goat biotin-SP (Jackson ImmunoResearch) for 1 h at room temperature. Sections were washed 5 times in 1X KPBS before being incubated in avidin-biotin-peroxidase complex (1:10, ABC Elite Kit, Vector Laboratories) for 1 h at room temperature. After rinsing sections 3 times in 1X KPBS and 3 times in 0.175M sodium acetate buffer, Iba1 or GFAP immunoreactivity was visualized with nickel sulfate enhanced 3,3′-diaminobenzidine (DAB) solution (2.0mg/10mL) containing 0.08% hydrogen peroxide in 0.175M sodium acetate buffer. Sections were incubated in the DAB solution for 15 min before rinsing 3 times with 0.175M sodium acetate buffer followed by 3 times in 1X KPBS. Sections were then mounted onto gelatin subbed slides, air dried, then dehydrated in a graded series of alcohols, and cleared with xylenes. Slides were then cover slipped with Permount mounting media. Brightfield

images of the slides were acquired on a Nikon Eclipse E800 microscope with a QImaging Retiga Exi CCD camera using 4X Plan-Apochromat N.A. 0.2 and 10X Plan-Apochromat N.A. 0.45 air objectives. For densitometry, background subtraction and thresholding were first performed on the images using ImageJ. Cell count analysis was performed using Cell Profiler 4.2.1 (Broad Institute) (Carpenter et al., 2006).

RT-qPCR

GT1-7 cells were seeded at a density of 2.5×10^5 in a 6-well dish. QIAzol (QIAGEN) reagent from the RNeasy Lipid Tissue Mini Kit (QIAGEN) was directly added onto the plates, removed using a cell scraper (Corning), and passed through a 27G needle. The concentration and purity of purified RNA were assessed spectrophotometrically using the NanoDrop ND-2000/2000c (ThermoFisher). RNA was only used if it had an A260/A280 ratio between 1.8–2.25. First-strand cDNA synthesis was performed using the iScript Reverse Transcription Supermix for RT-qPCR (BioRad) according to the manufacturer's protocol. RT-qPCR was performed using the Real-Time PCR System (LightCycler 96, Roche). Each reaction comprised of 0.5 μL of diluted cDNA, 5 μL FastStart Essential DNA Green Master Mix (Roche), and 10 μM primers in a final volume of 10 μL. The PCR cycling conditions were as follows: activation at 95°C for 900s; then 3-step amplification with 45 cycles of 95°C for 15s; 63°C for 15s; and 72°C for 60s. Cycling was followed by melt curve recording at 95°C for 10s; 65°C for 60s; and 97°C for 1s. Primer standard curves were performed to estimate the PCR efficiencies for each primer pair. Cycle threshold (Ct) values were determined by Lightcycler 96 application software. All qPCR reactions were run in triplicate with at least 3 biological replicates where each biological replicate represented each RNA extraction/cDNA synthesis. A mean Ct value was calculated for each primer pair and each experimental condition. Relative quantification of *Gnrh1* mRNA was performed using the 2-ΔΔCt method (Livak and Schmittgen, 2001). Data were normalized to the geometric mean of *Gadph* and presented as expression relative to a standard condition as indicated in the figure legends. *Tnfa* and *Il1b* were analyzed using pre-made mouse PrimePCR primer sets (Bio-Rad). *Gnrh1* and *Gapdh* primers were designed using sequences from previous studies. Primer sequences are as follows:

GnRH-F: 5′-GCTCCAGCCAGCACTGGTCCTA-3′;

GnRH-R: 5′-TGATCCACCTCCTTGCCCATCTCTT-3′ (Nuruddin et al., 2014);

GAPDH-F: 5′-GGCAAATTCAACGGCACAGT-3′;

GAPDH-R: 5′-GGGTCTCGCTCCTGGAAGAT-3′ (Wall et al., 2018).

GnRH ELISA

Cells were seeded at a density of 1×10^6 cells/well in a 6-well dish with DMEM (Corning) with 10% FBS (GE Healthcare) and 1% Pen Strep (ThermoFisher) overnight. Cells were then washed with PBS and supplemented with DMEM (Corning) with 1% Pen Strep (ThermoFisher) and 0.2% bovine serum albumin (Sigma). Media from cells were collected 4 h later. Samples were then centrifuged at 10,000 RPM for 20 min at 4°C. The supernatant was collected and stored at −80°C for GnRH ELISA (Cusabio, Inc.). ELISA was performed according to the manufacturer's directions.

GT1-7 CRISPR rescue

GT1-7 CRISPR cells were plated at a density of 1.0×10^6 in a 10-cm dish and transfected with CRISPR-resistant *Rnf216/Triad3* isoforms A and B (*Rnf216* Isoform A (GenBank ID: NM_080561.4) and *Rnf216/Triad3* Isoform B (GenBank ID: NM_207110.1)). Plasmids were created by using the gRNA sequences previously used for CRISPR A and B, changing the wobble position to create the target sequences for Isoform A and B (shown below) for mouse wildtype *Rnf216/Triad3*. Both sequences were cloned and inserted into the pcDNA3.1(+)-N-eGFP vector using SC1691 express cloning and the plasmids were made using SC1010 gene synthesis for mammalian cells (GenScript USA, Inc.). Both isoforms A and B were transfected into GT1-7 CRISPR control and B clones to create CRISPR Ctrl Rescue and CRISPR B Rescue using the standard Lipofectamine 3000 (Thermo Fisher) protocol. Briefly, 2.5μg of each Isoform plasmid DNA was mixed with Lipofectamine 3000 reagents which were added to the CRISPR cell clones and incubated for 6–8 h before replacing with fresh media. Cells were analyzed 24 h later with quantitative PCR for *Gnrh1* to assess if

knockout phenotypes were restored. The *Rnf216/Triad3* CRISPR resistant targeting sequences were as follows (wobble mutations in bold):

Isoform A- 5′-**A**AATAA**T**TT**CCC**A**T**GT**C**ATCG**C**-3′;

Isoform B- 5′-TC**T**GT**G**GA**C**GATCA**A**CT**G**AT**A**-3′.

Subcellular fractionation

The fractionation of GT1-7 cells was adapted from Abcam (https://www.abcam.com/protocols/subcellular-fractionation-protocol). Each cell line was seeded at a density of 1×10^7 cells on a 10 cm dish. After the media was removed, ice-cold DPBS was added to the plates to wash off the remaining media and dead cells. 500μL of fractionation buffer (Abcam) was added and the cells were removed by scraping. Membrane, nuclear, cytoplasmic, and mitochondrial fractions were isolated according to the manufacturer's protocol. Cell fractions were stored at −80°C until processed. Cell fraction samples were thawed on ice and 10-20 μL of RIPA buffer (50mM Tris-HCl pH 8.0, 150mM NaCl, 1% NP-40, 0.5% sodium deoxycholate, 0.1% SDS) was added for 30 min with disrupting the pellet every 5 min and then centrifuged for 20 min at 14,000 rpm at 4°C. The soluble fraction was collected and 2XSDS sample buffer (10% 1M Tris-HCl pH6.8, 3% DTT, 4% SDS, 20% glycerol, 0.2% Bromophenol blue, 1:1000 dilution of β-Mercaptoethanol) was added to each protein sample and boiled at 95°C for 7 min before loading on an SDS-PAGE gel (see below). After protein transfer, membranes were blotted with Revert 700 total protein stain (LiCor) before blocking.

Western blotting

4-week-old male and female mouse tissue was thawed on ice and 300-500 μL of RIPA buffer was added and the tissue was homogenized using sterile pestles. The samples were then centrifuged at 14,000 rpm for 15 min at 4°C and the supernatant was collected for protein quantification. GT1-7 cells were prepared as stated previously in the subcellular fractionation section. The soluble fraction was collected and the protein concentration was determined using Pierce 660nM Protein Assay Kit (ThermoFisher). The samples underwent SDS-polyacrylamide gel electrophoresis and were transferred on nitrocellulose membrane (BioRad) for 1 h at 70 mV. The blots were incubated overnight at 4°C with blocking buffer (Intercept (TBS) blocking buffer, LiCor). Membranes were then probed with the following primary antibodies prepared in a 1:1 ratio of TBST (1X TBS, 0.1% Tween-20) and blocking buffer solution with 1:1,000 20% NaN₃: rabbit polyclonal anti-RNF216 (Bethyl Laboratories, 1:1,000), rabbit anti-KISS1R/GPR54 (Lifespan Biosciences, 1:600), rabbit anti-GNRHR (Lifespan Biosciences, 1:600), rabbit anti-Arc (Synaptic Systems, 1:1,000), rabbit anti-GFP (Fisher, 1:1000), or mouse anti-β-Actin (Genetex, 1:3,000) and were incubated overnight at 4°C. The blots were then washed 3 times in dH20. The following secondary antibody dilutions were prepared in a 1:1 ratio of TBST (1X TBS, 0.1% Tween-20) and blocking buffer solution with 1:2,000 20% SDS: IRDye 680RD Goat anti-Mouse IgG (H+L) (Li-COR, 1:20,000) and IRDye 800CW Goat anti-Rabbit IgG (H+L) (Li-COR, 1:15,000) and were incubated for 1 h at room temperature. Blots were washed 2 times in TBST, 1 time in dH₂O, and imaged using the Odyssey CLx Imaging System (LI-COR) with a resolution of 169 μm, medium quality, and a 0 mm focus offset. Images were processed using the Gel Analysis tool in ImageJ using individual channels. Briefly, boxes were drawn around each band. Once the lanes were labeled and plotted, the area of the peaks was selected and measured. For each blot, proteins of interest were normalized to a loading control.

Transferrin receptor uptake in neurons

WT primary rat hippocampal neurons from PN Day 0 pups were transfected at DIV 15-17 with either GFP alone or GFP in combination with pRK5FLAG-Triad3A-WT or-CA (Catalytic inActive) plasmids, and scramble- or *Triad3A*-shRNAs using Lipofectamine 2000 (Thermo Fisher) (Mabb et al., 2014). Transferrin receptor uptake assay was performed 48 h following transfection as previously described (Blanpied et al., 2003).

Calcium imaging

GT1–7 CRISPR cells were plated on glass cover-slips (22 mm diameter) coated with poly-D-lysine (100 μg/mL) at a density of 30,000 cells/coverslip. The cells were maintained as previously described under the cell culture section. The next day, cells were transfected with CMV-R-GECO1.2 (Addgene #45494) (Wu et al., 2013) using Lipofectamine 3000 as described above in the generation of control and *Rnf216/Triad3* CRISPR clones section. During imaging, cells were shifted to ACSF solution (mM) containing 118 NaCl, 3

KCl, 0.5 CaCl₂, 6 MgCl₂, 5 HEPES, 25 NaHCO₃, 11 D-glucose, pH 7.3. Cells were imaged in live conditions using highly inclined and laminated optical sheet (HILO) microscopy on a Nikon Ti-E inverted microscope equipped with a Nikon 100× TIRF objective and an Andor IXon Ultra 897 EMCCD camera at an imaging speed of 1 frame per second (Reddish et al., 2021). A CW 561 nm laser (Oxxius) was used for exciting the fluorophore and a Quad-Band filter set (TRF89901v2, Chroma) was used for rejecting the fluorescence background. Calcium signals were acquired after measuring ΔF/F using the "delta F up function" and the "F div F0" function in Image J (FIJI). Values were normalized to one using (x – min(x)) / (max(x) – min(x)). Peak amplitudes were extracted using "findpeaks" in Matlab (The MathWorks, Inc.), which were defined as 2 standard deviations above the mean fluorescence.

QUANTIFICATION AND STATISTICAL ANALYSIS

Graph Pad (version 8.0) was used for all graphs. Unpaired *t*-test, One-way ANOVA, and Two-way ANOVA with multiple comparisons were applied for statistical analysis. Bonferonni and Tukey's tests were used for comparing group means only when a significant F value was determined for ANOVA tests. In experiments where parametric assumptions cannot be applied, non-parametric tests (i.e. Mann-Whitney-U) were utilized or Chi-square were used for categorical/nominal data. For all comparisons, significance was set at *$p \leq 0.05$, **$p \leq 0.01$, ***$p \leq 0.001$, and ****$p \leq 0.0001$ for 95% confidence intervals. Data presented in figures and tables are means (+ or $\pm$ SEM). Statistical details of experiments (e.g. tests used, exact value of n, what n represents, definition of center, and dispersion/precision measures) can be found within the figure legends and methods section. Image acquisition, analysis, and specific software details can be found within the figure legends and in the methods section.